The Meteoritical Society

Meteoritics & Planetary Science 51, Nr 12, 2366–2386 (2016)
doi: 10.1111/maps.12729

Global variations in regolith properties on asteroid Vesta from Dawn's low-altitude mapping orbit

Brett W. DENEVI[1*], Andrew W. BECK[1], Ecaterina I. COMAN[1,2], Bradley J. THOMSON[3], Eleonora AMMANNITO[4,5], David T. BLEWETT[1], Jessica M. SUNSHINE[6], Maria Cristina DE SANCTIS[4], Jian-Yang LI[7], Simone MARCHI[8], David W. MITTLEFEHLDT[9], Noah E. PETRO[10], Carol A. RAYMOND[11], and Christopher T. RUSSELL[5]

[1]The Johns Hopkins University Applied Physics Laboratory, Laurel, Maryland 20723, USA
[2]Department of Earth and Planetary Sciences, Washington University, St. Louis, Missouri 63130, USA
[3]Center for Remote Sensing, Boston University, Boston, Massachusetts 02215, USA
[4]Istituto di Astrofisica e Planetologia Spaziali, INAF, 00133 Rome, Italy
[5]Institute of Geophysics and Planetary Physics, University of California, Los Angeles, California 90095, USA
[6]Department of Astronomy, University of Maryland, College Park, Maryland 20742, USA
[7]Planetary Science Institute, Tucson, Arizona 85719, USA
[8]NASA Lunar Science Institute, Boulder, Colorado 80302, USA
[9]Astromaterials Research and Exploration Science Division, NASA Johnson Space Center, Houston, Texas 77058, USA
[10]NASA Goddard Space Flight Center, Greenbelt, Maryland 20771, USA
[11]Jet Propulsion Laboratory, California Institute of Technology, Pasadena, California, USA
[*]Corresponding author. E-mail: brett.denevi@jhuapl.edu

(Received 17 June 2015; revision accepted 22 July 2016)

Abstract–We investigate the depth, variability, and history of regolith on asteroid Vesta using data from the Dawn spacecraft. High-resolution (15–20 m pixel^{-1}) Framing Camera images are used to assess the presence of morphologic indicators of a shallow regolith, including the presence of blocks in crater ejecta, spur-and-gully–type features in crater walls, and the retention of small (<300 m) impact craters. Such features reveal that the broad, regional heterogeneities observed on Vesta in terms of albedo and surface composition extend to the physical properties of the upper ~1 km of the surface. Regions of thin regolith are found within the Rheasilvia basin and at equatorial latitudes from ~0–90°E and ~260–360°E. Craters in these areas that appear to excavate material from beneath the regolith have more diogenitic (Rheasilvia, 0–90°E) and cumulate eucrite (260–360°E) compositions. A region of especially thick regolith, where depths generally exceed 1 km, is found from ~100–240°E and corresponds to heavily cratered, low-albedo surface with a basaltic eucrite composition enriched in carbonaceous chondrite material. The presence of a thick regolith in this area supports the idea that this is an ancient terrain that has accumulated a larger component of exogenic debris. We find evidence for the gardening of crater ejecta toward more howarditic compositions, consistent with regolith mixing being the dominant form of "weathering" on Vesta.

INTRODUCTION

The Dawn spacecraft spent nearly 14 months in orbit around 4 Vesta, mapping the asteroid with a Framing Camera (FC), a Visible and InfraRed mapping spectrometer (VIR), and a Gamma Ray and Neutron Detector (GRaND) (Russell et al. 2012, 2013). These three instruments investigated the surface of Vesta, sampling depths ranging from the upper few micrometers of the surface (FC, VIR) to several decimeters (GRaND). As such, most of the remote sensing data collected by Dawn come from the vestan regolith.

On airless bodies, regolith is a surface/near-surface layer of fragmental debris ranging in particle size from

dust grains (micrometers) to house-sized boulders (tens of meters) that is produced mainly by impact events of all sizes. Regolith is sometimes distinguished as being more heavily gardened than the underlying "megaregolith," ejecta deposits or brecciated and fractured debris produced by large impact basins (Hartmann 1973). However, determining where the transition from regolith to megaregolith to bedrock occurs is not straightforward in ancient regions where impacts have pulverized and fractured the surface to great depth (Cintala and McBride 1995). We adopt a definition of regolith as the layer of fragmental debris overlying a more coherent substrate, similar to that of Oberbeck et al. (1973). Regolith is thus a mixture of local material comminuted by impacts more or less in situ, and material excavated by distant impacts, whose ejecta can be scattered hundreds of kilometers, meaning globally in the case of Vesta (285 km equatorial radius [Jaumann et al. 2012]). Knowledge of the origin, depth, and mobility of the vestan regolith is thus of consequence for a contextual understanding of results from each of Dawn's instruments.

All asteroids visited by spacecraft to date have shown evidence for a surficial layer of regolith (e.g., Helfenstein et al. 1994, 1996; Veverka et al. 2001; Saito et al. 2006; Sierks et al. 2011a) that can be locally deep (tens to hundreds of meters deep in places on Eros [Robinson et al. 2002]). Regolith on asteroids also displays enhanced mobility due to seismic shaking (e.g., Cintala et al. 1978; Richardson et al. 2005), indicating that regolith can act as a homogenizing surface layer, muting any subsurface compositional variation and leading to rapid degradation of surface features formed in loose material. There is clear evidence for a widespread fine-grained regolith on Vesta with particle sizes similar to those of the Moon (Pieters et al. 1993; Hiroi et al. 1994; Jaumann et al. 2012; Schröder et al. 2013; Capria et al. 2014). Initial results from Dawn find the regolith to be 800 ± 100 m deep in one location (the ejecta blanket of Lepida crater) by examining the infilling of small craters (Jaumann et al. 2012). Portions of Vesta's equatorial and northern regions have crater size–frequency distributions that may be at or near saturation, suggesting that these regions of the surface record much of the asteroid's earliest history (Marchi et al. 2012; Ruesch et al. 2014b), allowing substantial time for the growth of regolith. Large regions with elevated hydrogen content and relatively low albedo correspond to some of these highly cratered terrains, and are interpreted to be ancient regolith deposits that have accumulated substantial fractions of exogenic carbonaceous chondrite impactors over time (McCord et al. 2012; Prettyman et al. 2012; Reddy et al. 2012b). In contrast, the Rheasilvia basin occupies much of the southern hemisphere (diameter ~500 km) and may have formed as recently as 1 Ga (Marchi et al. 2012), although ages as old as 3.5–3.6 Ga have been proposed (Schmedemann et al. 2014). Thus, Vesta presents an opportunity to examine multiple surfaces on a single asteroid that may vary substantially in age: relatively old equatorial and northern regions versus a younger southern hemisphere.

Vesta's regolith poses an especially interesting puzzle because, despite evidence that some regions possess an ancient regolith, reflectance spectra indicate its surface has been much less altered by space weathering than the surface of the Moon (Matson et al. 1977; Burbine et al. 2001; Pieters et al. 2012; Blewett et al. 2016) or many other asteroids (e.g., Clark et al. 2002). Space weathering, as understood for the Moon, is the collection of physical (comminution, vitrification, agglutination) and chemical (reduction of ferrous iron to nanophase iron metal) changes that result from micrometeoroid bombardment and interactions with the solar wind (e.g., Pieters et al. 2000; Hapke 2001). The causes of Vesta's apparent lack of lunar-style space weathering are not known, but this leaves mixing and overturn of a mobile regolith as the dominant form of weathering on Vesta (Pieters et al. 2012).

Vesta is unique in that it is the likely source for the most voluminous set of materials from a known extraterrestrial body (Beck et al. 2015): the HED (howardite, eucrite, and diogenite) meteorite clan (McCord et al. 1970; Wisdom 1987; Binzel and Xu 1993). From broad to narrow, meteorite taxonomic grouping follows the progression clan, to group, to subgroup (Weisberg et al. 2006). The eucrite group of the HED clan consists of plagioclase and pyroxene basalts and gabbros, while the diogenite group consists of ultramafic cumulates. The most voluminous subgroups in the eucrite and diogenite groups are the basaltic eucrites and orthopyroxenitic diogenites, respectively. They represent distinct igneous layers on Vesta that formed during differentiation at ~4.565 Ga (Lugmair and Shukolyukov 1998), or ~2.3 Myr after CAI formation (Trinquier et al. 2008). The basaltic eucrites are thought to have formed as a volcanic crust on the vestan surface, while orthopyroxenitic diogenites formed as a deeper seated unit(s), either as a contiguous lower crustal layer, or in multiple crustal plutons. Cumulate eucrites, another eucrite subgroup, also formed at some depth beneath the basaltic eucrite crust. The howardite group consists of polymict breccias primarily containing clasts from the basaltic eucrite and orthopyroxenitic diogenite subgroups, as well as exogenic components such as clasts of carbonaceous chondrites (e.g., McSween et al. 2011; Mittlefehldt 2015).

Howardites are formed via impact at some point after vestan differentiation, and as such, they retain information about surface processes that have occurred on Vesta, including regolith formation and evolution. For example, howardites that resided in the regolith of Vesta for an extended period of time become enriched in noble gases. This howardite subgroup has been dubbed "regolithic howardites" or "gas-rich howardites" (Cartwright et al. 2013), as opposed to solar noble gas-poor "fragmental howardites" that come from areas beneath the surface, or megaregolith. Petrologic indicators, such as dark-matrix clasts, glass, and melt-matrix clasts have also been used to designate samples with a high regolithic grade (regolithic howardites) from those that do not share those characteristics (fragmental howardites) (Mittlefehldt et al. 2013).

Given the importance of regolith to studies of composition and space weathering, here we work to provide a more detailed understanding of the depth, evolution, mobility, and variability of regolith on Vesta. This is accomplished with morphologic studies using high-resolution Dawn FC image data (Sierks et al. 2011b), and comparisons with Vesta's photometric, thermal, and compositional properties. These results are evaluated both in the context of laboratory studies of howardite meteorites, and for what context they can provide for howardite formation. Finally, we seek a better understanding of the parent-body size dependence of regolith evolution, with Vesta providing an intermediate case between small asteroids that can be essentially gravity-bound piles of regolith and large airless terrestrial bodies such as the Moon and Mercury that have complex and diverse regolith processes.

DATA AND METHODS

Most methods for estimating regolith depth require reasonably high-resolution images, thus we focus our efforts on analysis of FC images acquired during Dawn's low-altitude mapping orbit (LAMO) of Vesta. This phase of Dawn's mission lasted just under 5 months and provided near-continuous FC clear-filter coverage of southern and equatorial regions from an average altitude of ~210 km. Latitudes above ~55°N were shadowed for the entirety of LAMO. FC images acquired during LAMO ranged in resolution from ~15–20 m pixel^{-1} and solar incidence angles (measured from the surface normal) were >45° with an average incidence angle of 57°, providing a high-quality data set for morphologic studies of Vesta's surface. Because of Vesta's irregular shape (over 40 km of relief relative to a biaxial ellipsoid of 285 × 229 km) and commonly steep slopes (up to 40°; Jaumann et al. 2012), we analyze FC images by overlaying them on a shape model and visualizing them in three dimensions using the Small Body Mapping Tool (SBMT) developed by Kahn et al. (2011). All features were mapped directly onto the Vesta shape model of Gaskell (2012) that was produced using stereophotoclinometry (Gaskell et al. 2008).

Methods to remotely characterize regolith depth were first developed for studies of the Moon, often using images from the Lunar Orbiter missions with equivalent resolutions of 1–2 m pixel^{-1} (Hansen 1970). Thus, classic methods, such as documenting variations in interior crater morphology that depend on regolith depth (Oberbeck and Quaide 1968; Quaide and Oberbeck 1968), are not possible using 15–20 m pixel^{-1} LAMO data. However, we adopt several methods used previously for the Moon and asteroids that can provide depth constraints, and taken together can provide a robust picture of Vesta's regolith. These morphologic methods include assessing the presence (or lack) of coherent material within a crater's ejecta; examining layering within crater walls; studying morphologic evidence for downslope movement and infilling of topographic lows with regolith; and documenting the preservation of small craters, formed mostly within the regolith, in different locations. We detail each of these methods and their results in the following sections.

We note here that all coordinates are given in the "Claudia" system of the Dawn team (Roatsch et al. 2012; Russell et al. 2012, 2013). An approximate conversion from this coordinate system to the International Astronomical Union system can be achieved by subtracting 150° from the longitude (see Roatsch et al. [2012] for precise corrections).

BLOCKY CRATER DISTRIBUTION

As each impact occurred on Vesta, depending on its size and the depth of the local regolith, the resulting crater either formed entirely within regolith, ejecting only fine-grained material that was already fractured and comminuted by previous impacts, or it penetrated through this surficial layer to more coherent material, leading to the excavation of boulders or blocks. Thus, in regions of thin regolith, craters whose depth of excavation is greater than the depth of the regolith will excavate blocks, whereas equivalent-sized craters will not excavate blocks in a region of thicker regolith. This straightforward scenario was first used to estimate regolith depth on the Moon using Surveyor I lander images (Rennilson et al. 1966), and we adopt it here with several important caveats. First, craters may excavate blocks from within the regolith or from the megaregolith, rather than from true bedrock. Craters that have excavated such material would lead to an

underestimate of regolith depth using this method. Second, while the block populations of fresh craters should be representative, a lack of blocks at older craters may be due to their burial within the regolith or destruction by impact or thermal processing (Hörz et al. 1975; Basilevsky et al. 2013, 2014; Delbo et al. 2014), and would lead to an overestimate in depth. Finally, the smallest boulder we can identify in FC images as a positive relief feature (sunlit side plus the shadow it casts) is ~20 m. Thus, it is unlikely that we can, in all cases, identify the smallest crater in a given region with blocky ejecta to constrain minimum regolith depth. Given these limitations, we map the locations and diameters of all craters on Vesta with any recognizable blocks in their ejecta. The size distribution of fragmental ejecta typically follows a power-law distribution (e.g., Shoemaker and Morris 1970), so while we often identify a relatively small number of blocks near the limit of resolution, there are likely to be many more blocks just below the limit of resolution. We compare the spatial distribution of blocky craters with broad regional trends in spectral reflectance and composition, with care to avoid overinterpretation of any single occurrence.

Examples of craters with block-rich ejecta are shown in Fig. 1. From all FC data acquired during LAMO, we identified 156 such craters in total, ranging in diameter from 680 m to 70 km. Boulders are associated with relatively fresh craters, consistent with burial and/or erosion of blocks at older craters (e.g., Hörz et al. 1975; Basilevsky et al. 2013, 2014). The maximum depth of origin of the blocky material exposed by these craters is approximately 10% of the transient crater diameter D_t (Croft 1981; O'Keefe and Ahrens 1987), and D_t is related to the observed crater diameter D by $D_t = 0.84D$ for simple craters such as those in this study (Melosh 1989). We thus focus on the distribution of blocky craters <12 km in diameter ($n = 122$), which provide information on the upper ~1 km of the regolith. Although LAMO images cover latitudes up to ~55°N, we find that shadows at latitudes greater than ~45°N are pervasive enough to obscure large portions of crater walls and interiors, and thus we use this as our northern study boundary. Below these latitudes, we find substantial variations in the distribution of blocky craters across Vesta. The largest concentration is between longitudes ~260–360°E, within and to the north of the Rheasilvia basin, and at equatorial longitudes from 0–90°E (Fig. 2). In comparison, a large equatorial region from ~100–240°E contains a relative dearth of block-rich craters <12 km in diameter (Fig. 2). Where blocky craters are seen within this region, most are found along the approximate rims of both the Rheasilvia and Veneneia

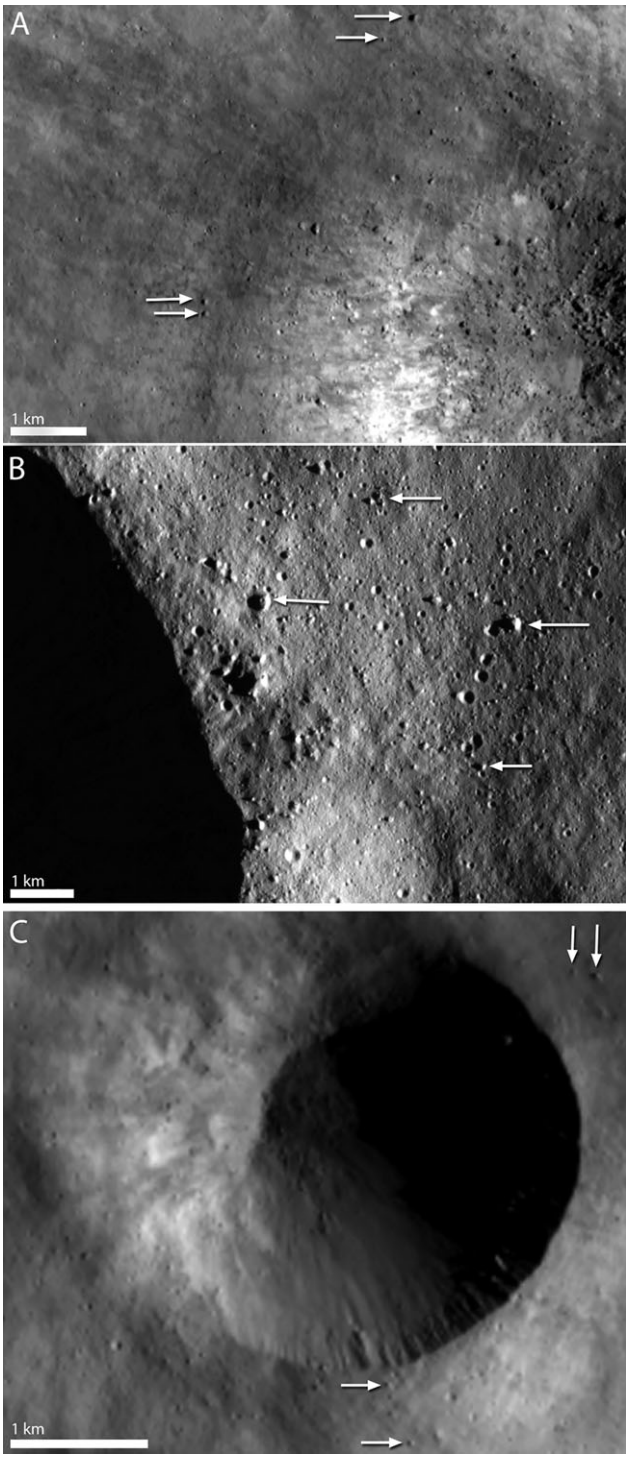

Fig. 1. Examples of blocks in Vestan crater ejecta. Arrows highlight selected boulders within the ejecta. A) Blocks surrounding a ~8.8 km diameter crater at 26.9°S, 220.2°E (image FC21A0014744_11354133949F1A). B) Blocks up to 250 m in the ejecta of a ~30 km crater, 22.3°N, 20.3°E (image FC21A3014333_11347133750F1A). C) Blocky ejecta of a crater ~3.3 km in diameter, 67.5°S, 127.5°E (image FC21A0015660_11361180456F1A). Illumination is from the east in each image.

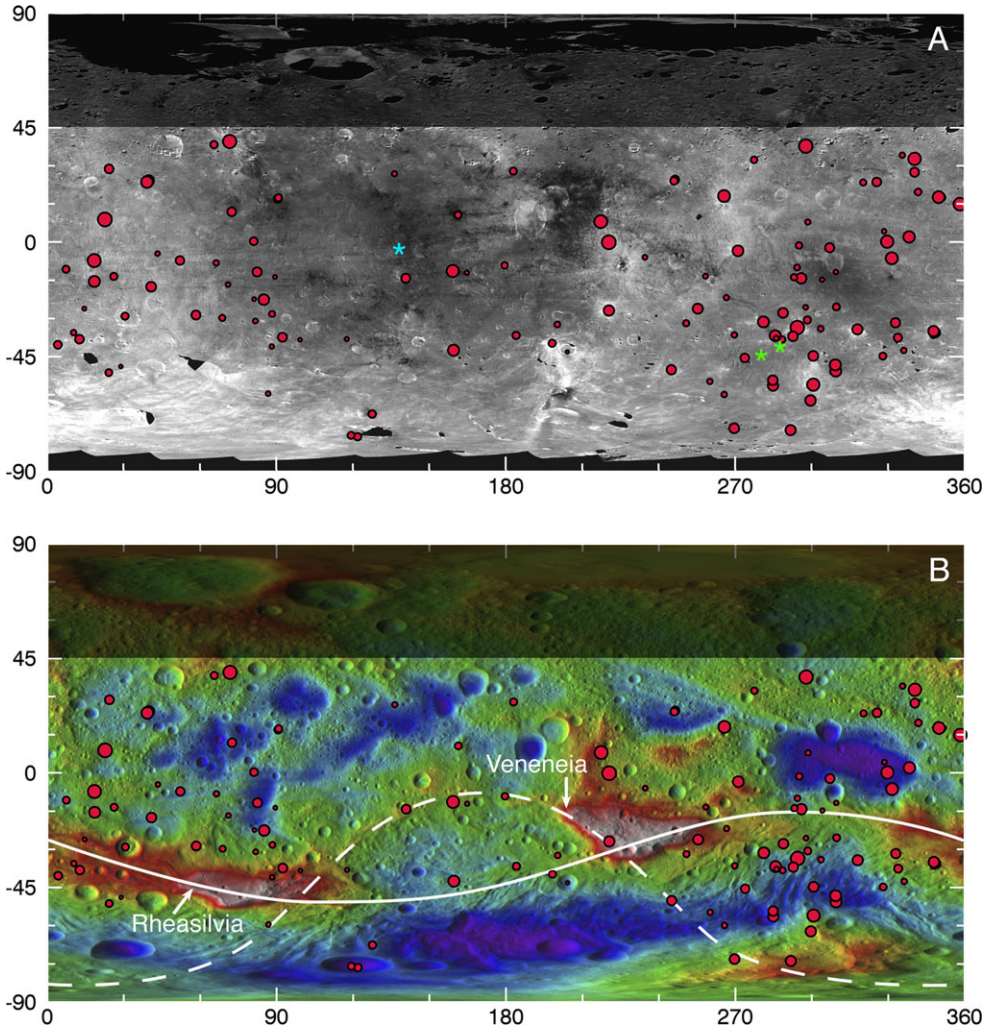

Fig. 2. The locations of craters smaller than 12 km in diameter that have excavated blocky material (red circles). The size of each circle is relative to the size of the crater indicated. A) FC normalized reflectance map of Vesta (reflectance stretched from values of 0.11–0.23). The locations where crater size–frequency distributions were assessed are indicated with blue (equatorial) and green (Rheasilvia) asterisks (see Fig. 6). B) Digital terrain model of Vesta (Gaskell 2012) shown relative to 285 × 285 × 229 km ellipsoid (scaled from −22.5 km [purple] to +19.5 km [white]). The approximate rims of the Rheasilvia (solid white line) and Veneneia basins (dashed white line) are shown. Latitudes above 45° were not included in this study due to pervasive shadows throughout the entirety of LAMO.

impact basins (Fig. 2B). (Veneneia is a ~400 km diameter basin of which approximately half was destroyed by the Rheasilvia impact event [Jaumann et al. 2012; Schenk et al. 2012]). The rims of these basins are marked by relatively steep scarps, likely to be local sources of near-surface competent material. Within Rheasilvia, a larger proportion of block-rich craters are found on the portion of the basin that does not overlap the Veneneia basin.

OBSERVATIONS OF CRATER WALLS

Many FC images reveal a spur-and-gully type erosional pattern or layering within crater walls (Fig. 3) (Krohn et al. 2014; Scully et al. 2015). These can range from spurs interspersed with regions of downslope mass wasting and well-defined talus deposits that occur along a large portion of the crater wall (Figs. 3A and 3B), to an isolated spur or thin horizontal layer or bench that can be traced along a relatively constant depth within the crater (Fig. 3C). Spurs of resistant material are far more common than craters with evidence for layering of materials with different mechanical properties. Each of these instances indicates material resistant to erosion is exposed within the crater wall near the surface. However, those resistant materials need not be bedrock; similar features on Mars have been interpreted to have the strength of moderately cohesive debris, mechanically

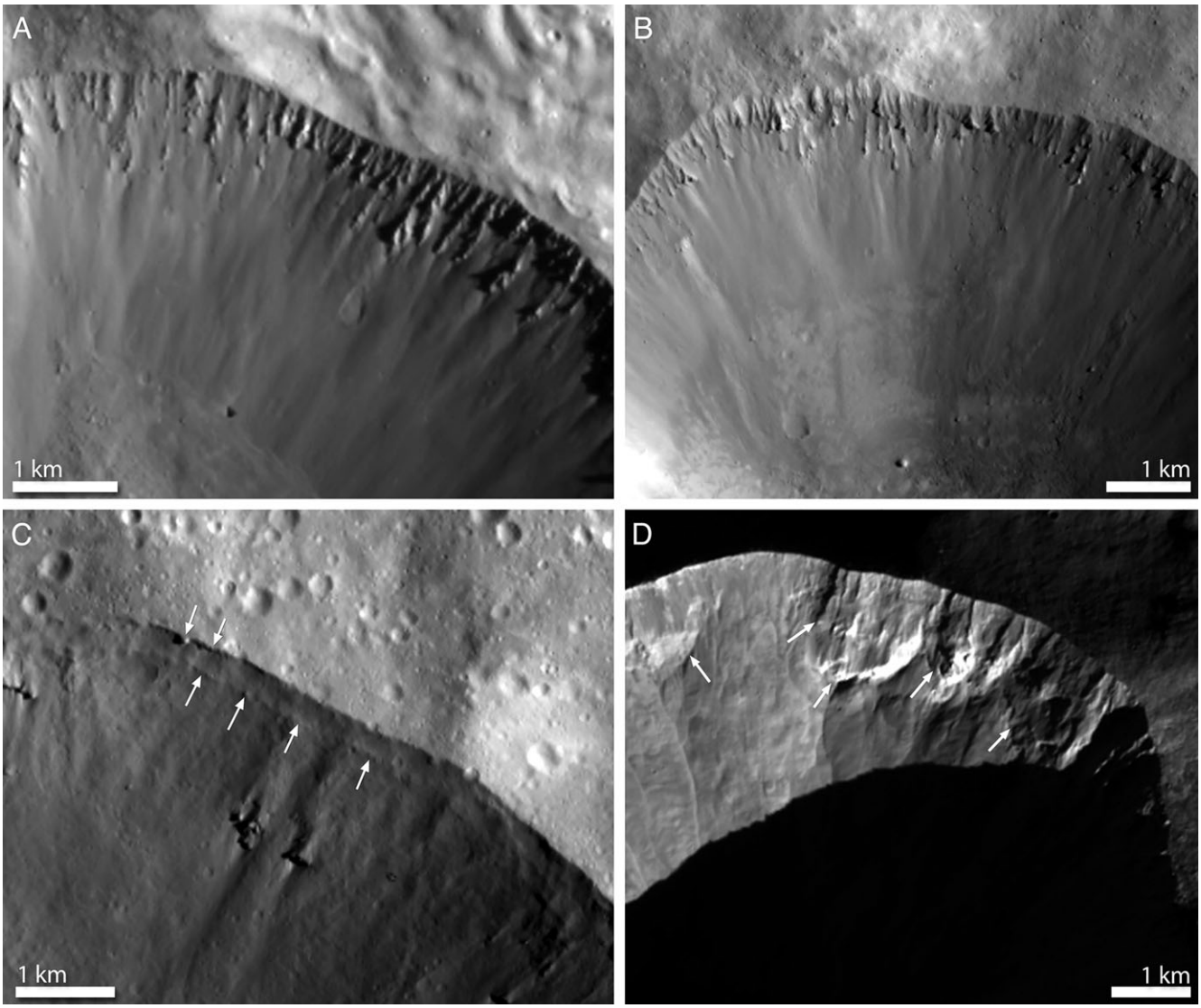

Fig. 3. Examples of exposures of coherent material within vestan crater walls. A) Spur-and-gully–type features in the wall of a ~15 km crater centered at 58.7°S, 200.7°E (image FC21A0014923_11355163605F1A). B) Spur-and-gully–type features in the wall of a ~12 km crater centered at 32.8°S, 294.8°E (image FC21A0015762_11363045345F1A). C) A resistant layer ~250 m below surface (lower arrows) and a possible resistant layer and overhang of material at the surface (upper arrows). Crater is ~22 km in diameter, scene centered at 40.0°S, 205.5°E (image FC21A0015710_11361221112F1A). D) Competent material just below the rim of the 10.5 km crater Arruntia at 40.0°N, 72.1°E (image FC21B0017965_12033014506F1D).

analogous to glacial till (Sullivan 1992). Here we examine the distribution of such features, which can provide information on layering within the regolith or a transition to more cohesive material below (megaregolith or in some cases possible bedrock).

In LAMO images, we identified 79 craters with these erosional patterns and recorded their sizes and locations (Fig. 4). Nearly 70% of these craters also have blocks in their ejecta, but the distribution of craters with resistant material in their walls is more widespread than the <12 km blocky craters. Spur-and-gully features found within smaller craters are more likely to be related to competent material found at relatively shallow depths, although there is no straightforward way to assess more than relative trends for regolith depth due to uplift of material during the impact event and slumping of material within the crater that may cover features. Still, examining the same size range used for blocky craters (<12 km in diameter, $n = 46$) shows that a high concentration is again found within the Rheasilvia basin, largely outside of the area that overlaps with the Veneneia basin (Fig. 4). In addition, many of the craters with spurs are those that formed on the rims of larger craters or on local topographic highs.

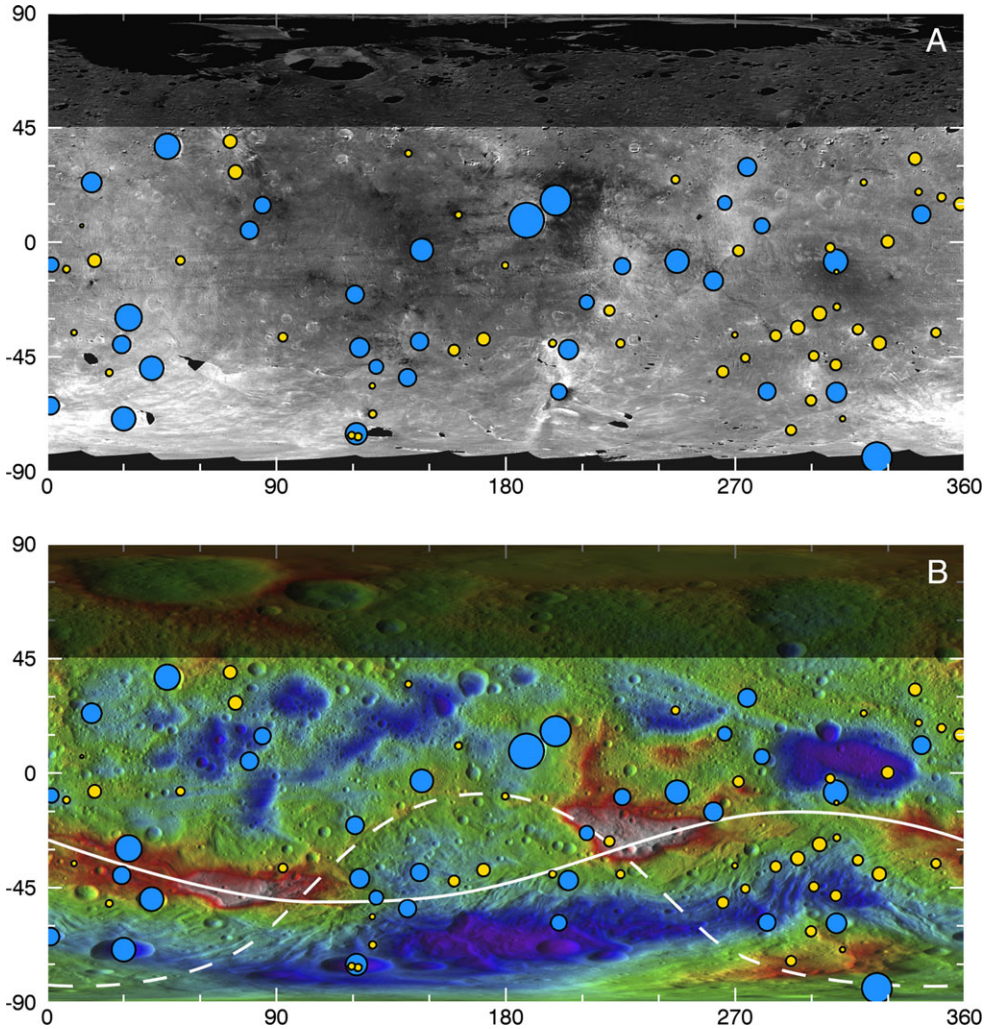

Fig. 4. Locations of craters that display spur-and-gully–type features in their walls; blue circles indicate host craters ≥12 km in diameter, yellow circles show craters <12 km in diameter. Symbol size is proportional to the host crater diameter. Underlying maps are the same as shown in Fig. 2; approximate Rheasilvia (solid white line) and Veneneia (dashed white line) basin rims are indicated.

For example, the 10.5 km diameter crater Arruntia (Fig. 3D), which has been interpreted to be rich in olivine (Ammannito et al. 2013a; Ruesch et al. 2014a; Palomba et al. 2015) or mixtures of low- and high-Ca pyroxene (Combe et al. 2015), abuts a region of higher topography to its north, which may be the source of more coherent material exposed in its crater walls.

Such crater wall features are rare on other asteroids. On Eros, only three craters with "hints" of layering or evidence of a strength discontinuity were found (Robinson et al. 2002), and none have been identified on other asteroids for which images of comparable resolution exist (i.e., Itokawa, Toutatis, and Ida). Resistant spurs are commonly seen in craters that formed in the lunar maria, and in such cases are often found near-continuously below the crater rim (Fig. 5A), in contrast to Vesta where spurs are typically observed on only a portion of the crater. In the lunar highlands, spurs are also observed on crater walls, but with less frequency. For fresh lunar highland craters that do exhibit spurs on their walls, they often have only limited exposures (e.g., Fig. 5B). Several of the highland craters with spurs are found on the continuous ejecta or rims of large basins such as Orientale or Moscoviense (Figs. 5C and 5D).

SMALL CRATER POPULATIONS

The population of small (less than ~300 m) craters provides another means to compare regolith in one region to another, as the density of small craters has been shown to be sensitive to regolith depth. For

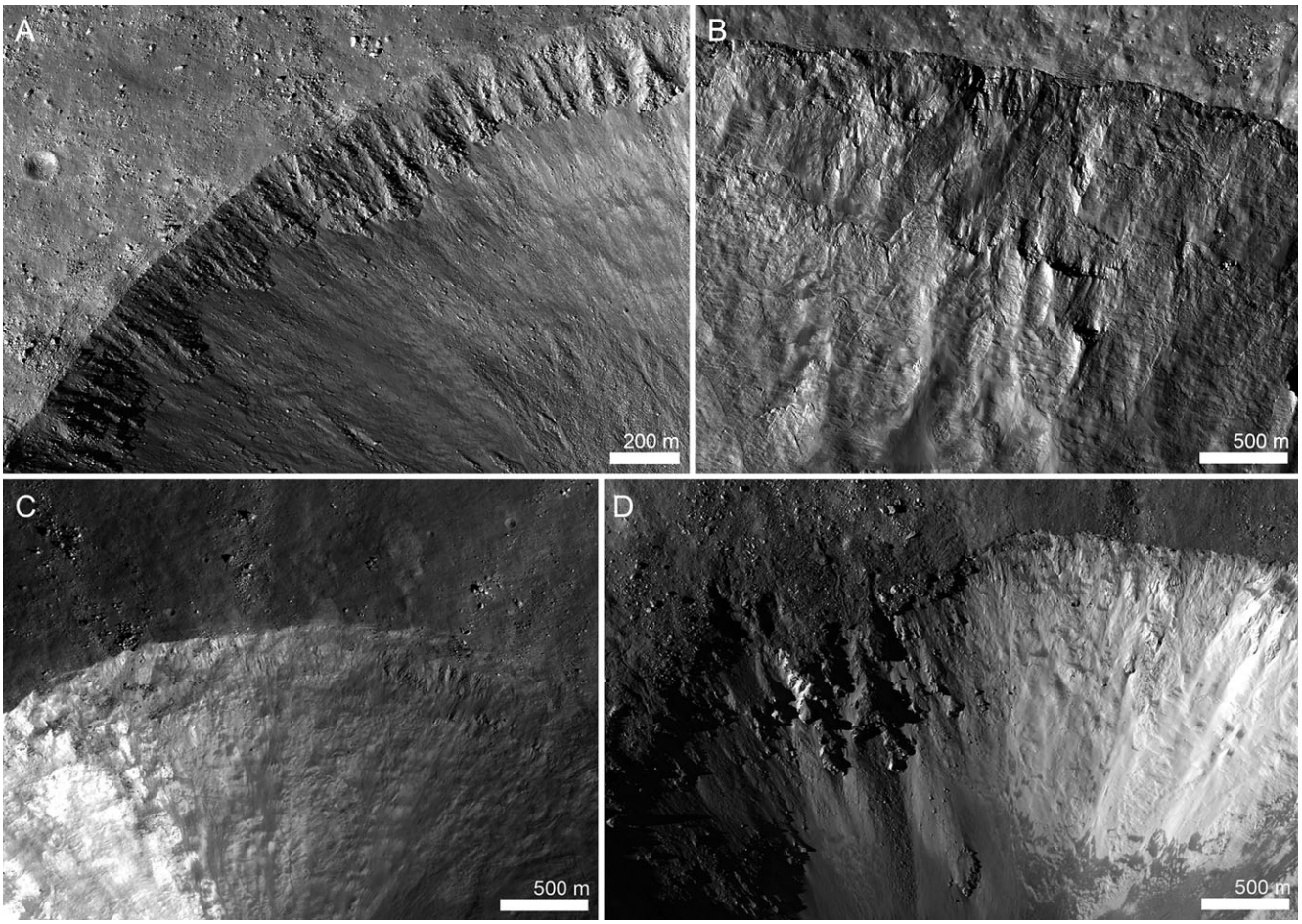

Fig. 5. Lunar craters with spur-and-gully–type erosion. A) Lichtenberg B (33.29°N, 298.40°E, LROC NAC image M120257109L), a lunar mare crater that displays coherent material nearly continuously below its rim. B) Crater Byrgius A (24.26°S, 296.2°E, image M1121649062R) in the highlands; here spurs are found in only portions of the wall. C) A crater just outside of the Moscoviense basin (32.75°N, 143.70°E, image M151936511R). D) A crater on the continuous ejecta deposit of the Orientale basin (3.41°N, 259.74°E, M1127782730R). While craters in the lunar maria are likely to expose bedrock, those in the highlands and on the ejecta of large basins likely expose coherent material within the regolith or megaregolith.

example, the lunar maria have substantially higher densities of small craters as compared to the older highlands, and Eros and Gaspra have been noted to have decreased crater densities below 200 m (Trask and Rowan 1967; Carr et al. 1994; Veverka et al. 2001; Robinson et al. 2002). This seemingly counterintuitive relationship of fewer small craters on older surfaces is attributed to the preferential degradation of craters that formed largely within the weakly coherent regolith of older regions, that also exhibit higher average slopes (Carr et al. 1994; Robinson et al. 2002; Wilcox et al. 2005; Fa et al. 2014).

We selected two representative areas and quantified the crater size–frequency distribution of each by recording the diameter and location of each crater within the region. The first location has an area of 110 km^2 and is centered at 2°S, 138°E within the low-albedo equatorial region identified as having a low density of blocky craters (Fig. 2). FC images of the area have an average native pixel scale of 19 m and average incidence angle of 51°. The second region is a combination of two nearby locations within the Rheasilvia basin at 44°S, 280°E and 40°S, 288°E with a combined area of 181 km^2. These areas were selected to avoid the steepest slopes within Rheasilvia. FC images in these areas have an average native pixel scale of 21 m and average incidence angle of 48°. These slight differences in incidence angle and native image resolution are unavoidable given the differences in latitude and spacecraft altitude over the two regions, but we have selected areas that minimize these differences as much as possible. All images were orthorectified and mosaicked to a common pixel scale. At the resolution of these images, crater densities

should be reliable for diameters of approximately 100 m and greater.

The crater size–frequency distributions are presented as both unbinned cumulative histograms and standard R plots, where the cumulative population is shown with root-two binning and normalized to slope of –3 (Crater Analysis Techniques Working Group 1979). As expected, for crater sizes larger than ~400 m, the equatorial region has a higher density of craters than does the region within the Rheasilvia basin (Fig. 6), consistent with the older inferred age of the equatorial region (Marchi et al. 2012). For crater diameters below ~400 m, these trends cross, and a higher density of craters smaller than this limit is observed within the Rheasilvia basin (Fig. 6A).

We compared our crater size–frequency distributions for Vesta to those of two lunar regions, a mare location in western Oceanus Procellarum (31.8°N, 282.3°E) and a location in the lunar highlands (31.5°N, 250.8°E). The crater populations were assessed for areas of 100 km^2 using mosaics from the Kaguya Terrain Camera (Haruyama et al. 2008) as compiled by Isbell et al. (2014). Terrain Camera data have a nominal resolution of 10 m $pixel^{-1}$ from an altitude of 100 km; we reduced the pixel scale to match that of the Dawn FC data.

The lunar mare and highland regions show trends comparable to those of the two regions on Vesta; relative to the lunar mare, the older lunar highlands have a higher density of craters at diameters larger than ~300–400 m, but have a lower density at smaller diameters (Figs. 6C and 6D). However, at small diameters, the variation between the older equatorial region and Rheasilvia on Vesta is smaller than the observed differences between the lunar mare and highland populations.

Our lunar crater size–frequency distributions compare favorably to those of Robinson et al. (2002) for lunar mare and highland regions. That work also examined the small crater populations of several regions on Eros (near Psyche and Himeros craters, and in Shoemaker Regio). The small-crater populations in both regions on Vesta are similar to those near Psyche and Himeros, but substantially higher in density than observed at Shoemaker Regio, an area noted for its especially thick and unconsolidated layer of regolith (Robinson et al. 2002).

REGOLITH MOBILITY AND INFILLING

As craters degrade, their uplifted rims erode and their interiors shallow due to infilling regolith produced or mobilized by nearby impacts (Shoemaker et al. 1969; Soderblom 1970). Craters that are heavily degraded and nearly filled with regolith are common on Vesta, suggesting local infilling with tens to hundreds of meters of regolith (e.g., Figs. 7A and 7B). While some craters appear to be affected by typical long-term degradation and infilling by numerous local impacts, others show evidence for infilling dominated by a single impact event. This second category often displays a scoured surface with an evident flow direction, and ejecta flow lobes that terminate on the up-slope side of filled craters (Figs. 7A and 7B); the source can often be traced to a nearby recent impact (Williams et al. 2013). These craters demonstrate the stochastic nature of local regolith development, where a single large event can dominate a region.

Abundant evidence is found for the downslope movement of regolith, forming large slumps, or smaller debris aprons (Jaumann et al. 2012; Williams et al. 2013; Krohn et al. 2014). Lower reflectance (relative to surroundings) talus deposits are often found on slopes (e.g., Figs. 7C and 7D), although in some cases the downslope movement of materials does not expose areas of higher than average reflectance, in contrast to typical deposits on the Moon (e.g., Figs. 5C and 5D), Eros, and Lutetia (Murchie et al. 2002; Thomas et al. 2002; Sierks et al. 2011a). In many cases, both low- and high-reflectance materials are observed as streaks on crater walls, interpreted as exposures of materials of differing composition rather than varying levels of lunar-style space weathering (Pieters et al. 2012).

DISCUSSION

Based on the distribution of blocky craters, we interpret the observations presented here to indicate that Vesta possesses a global regolith, the thickness of which is variable but often exceeds 1 km. These results are consistent with the low average thermal inertia values for Vesta (Capria et al. 2014) that suggest a global layer of fine-grained regolith and low photometric roughness values around even relatively fresh impact craters, implying relatively rapid smoothing of the regolith (Schröder et al. 2013). However, it is clear that the vestan regolith has not been homogenized to the extent observed on smaller asteroids. Although we see some evidence for the preferential degradation of small craters (Fig. 6), they are better preserved than on smaller asteroids such as Eros (Robinson et al. 2002; Richardson et al. 2004; Thomas and Robinson 2005) and Itokawa (Saito et al. 2006; Hirata et al. 2009) where seismic shaking is thought to be an important process for removing small craters (e.g., Richardson et al. 2005). The higher rate of degradation of small craters on these smaller bodies is consistent with individual impacts resulting in seismic

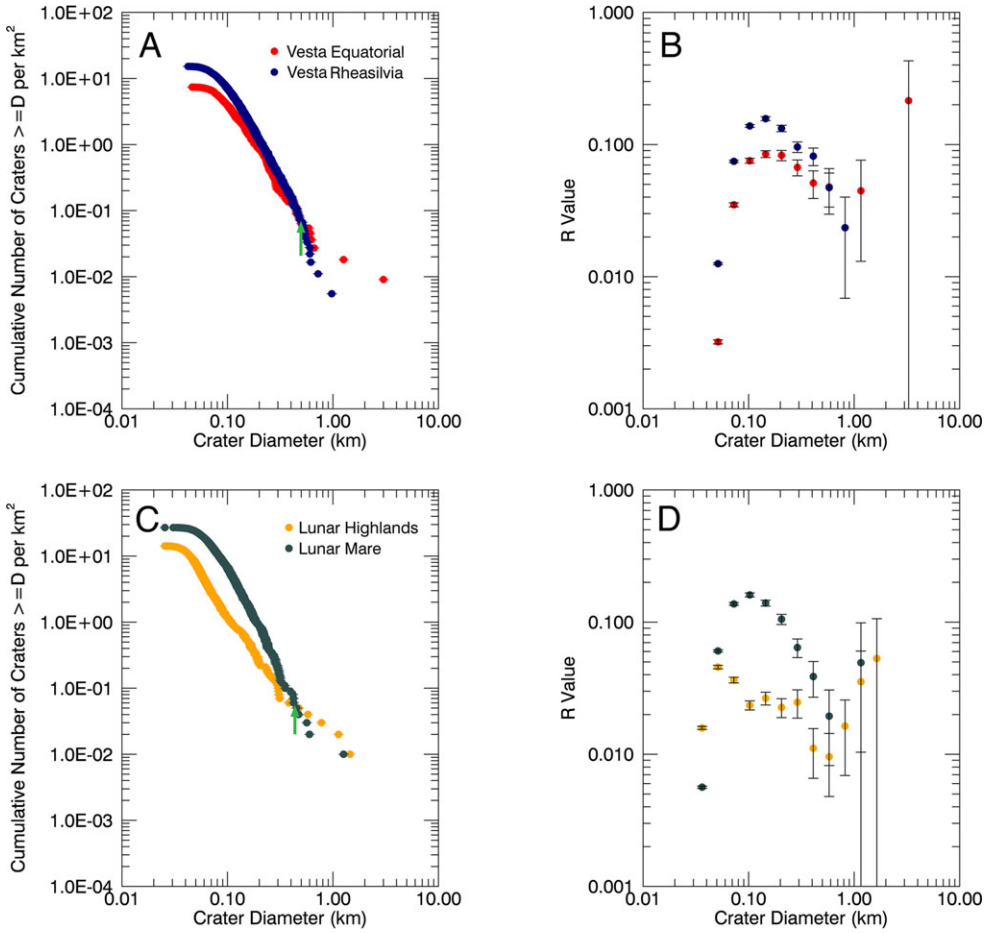

Fig. 6. Crater size–frequency distributions for two areas on Vesta (within Rheasilvia: blue, 44°S, 280°E; equatorial: red, 2°S, 138°E) and on the Moon (lunar mare: gray, 31.8°N, 282.3°E; lunar highlands: yellow, 31.5°N, 250.8°E). The unbinned cumulative histograms are shown in panels A and C for Vesta and the Moon, respectively, and the equivalent R-plots are shown in panels B and D. In comparison to younger areas (Rheasilvia, lunar mare), the density of craters in the older areas (equatorial Vesta, lunar highlands) is higher at large diameters and lower at small diameters; green arrows indicate the crossover point.

shaking having global surface-modifying effects only on asteroids smaller than ~70–100 km (Richardson et al. 2005). The differences between the small crater populations in the two regions of Vesta are smaller than the differences between the lunar mare and highlands regions we examined (Figs. 6C and 6D); this may be due to the high average slopes on Vesta (Jaumann et al. 2012), which promote degradation of small craters even in areas of relatively thin regolith.

The broad regional heterogeneities observed on Vesta in terms of albedo and composition extend to the physical properties of the upper ~1 km of the surface. The relative frequency of features indicative of competent material below the surface (blocks in ejecta, erosion-resistant material in crater walls) and the disparities in the preservation of small craters suggests differences in the thickness of regolith that are controlled both by the large-scale geologic history of the region in addition to local variability that results from the stochastic nature of impact cratering.

Longitudes extending from ~260°E to 90°E have a higher concentration of craters <12 km in diameter that have excavated blocks (Fig. 2), more craters with erosion-resistant material exposed within their walls (Fig. 4), and a higher concentration of small craters than elsewhere on the asteroid. Each of these characteristics is consistent with a regionally thinner regolith depth than average Vesta. The excavation depth of the craters that have ejected blocks suggests the thickness of the regolith in this region is often less than 1 km. This is consistent with results from crater size-frequency distributions near Lepida crater (307°E, 16°N) predicting a regolith depth of ~0.8 km in that area (Jaumann et al. 2012).

The portion of this region from ~260–360°E has a larger number of blocky craters and small craters with

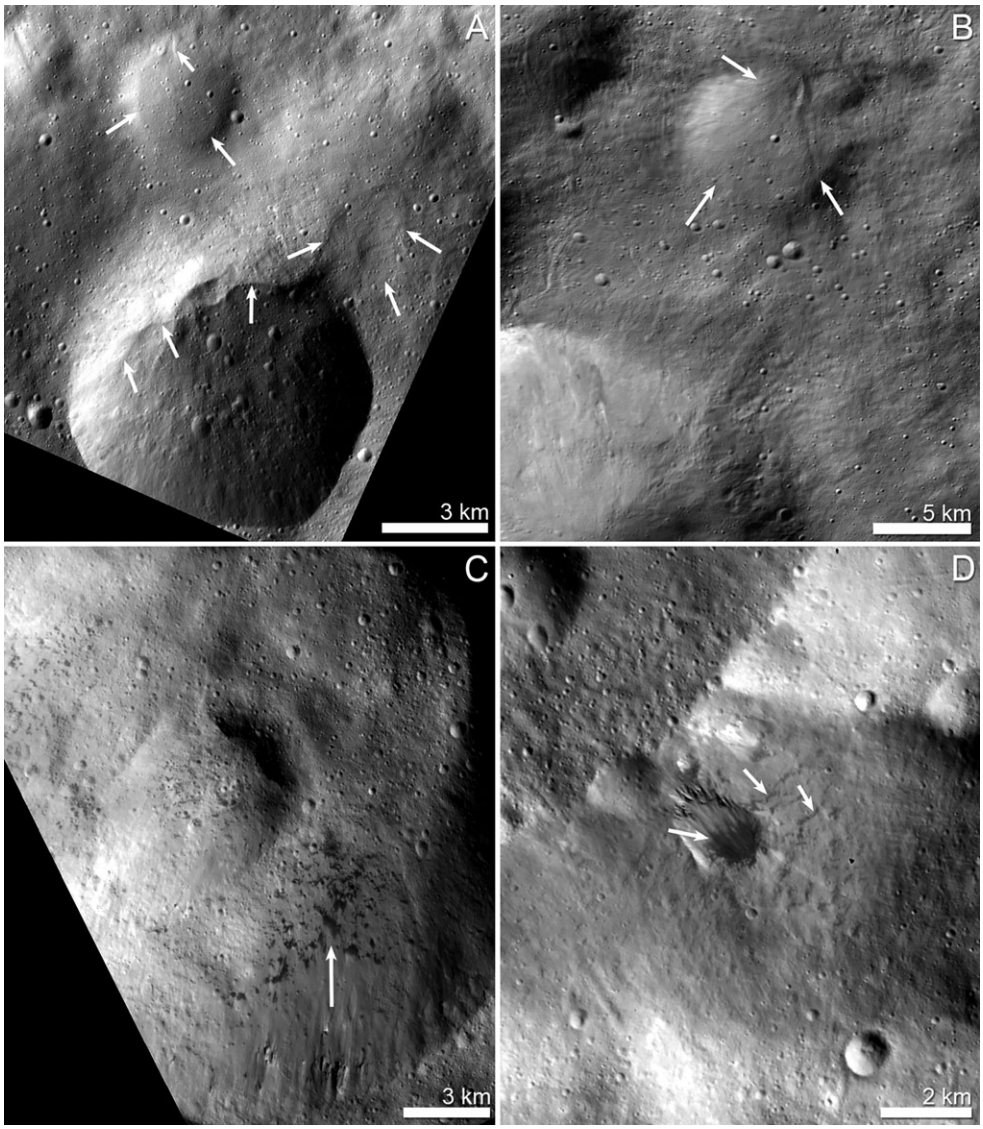

Fig. 7. Examples of regolith infilling and downslope movement on Vesta. A) Infilling of craters by ejecta from a nearby crater. Scene centered at 6°S, 332°E, image FC21B0026079_12111164145F1A. B) Infilling of an 8 km crater. Scene centered at 30°N, 15°E, image FC21B0018657_12038062748F3D. C) Downslope movement of material that does not expose high-reflectance material on the crater wall, in contrast to craters on the Moon, Eros, and Lutetia. Scene centered at 60°S, 311°E, image FC21A0014867_11354225647F1A. D) Downslope movement of materials that do not expose areas of high-reflectance on the steep slopes. Scene centered at 57°S, 127°E, image FC21A0015657_11361175641F1A.

resistant material in their walls within the Rheasilvia basin; from 0–90°E these features are largely seen to the north of the basin. The nonuniform distribution of blocky craters within Rheasilvia may suggest the regolith properties are controlled by the overlapping histories of the Veneneia and Rheasilvia impacts. Where Rheasilvia overprints the older basin Veneneia, just three craters that excavate blocks are observed, aside from those found along Rheasilvia's rim scarp (Fig. 2B). This is compared to over 10 times as many block-rich craters in the portion of Rheasilvia not overlapping Veneneia. This difference in distribution is consistent with the surface affected by both impacts being substantially more fractured and fragmented than the areas affected by Rheasilvia alone.

Many craters that expose competent material are found on topographic highs such as the Rheasilvia and Veneneia rim scarps. Exposures of topographic highs surrounded by relatively steep slopes may be the most likely regions in which true bedrock could be encountered, as downslope movement of regolith would leave high-standing areas with a thinner fragmental

covering. Such may be the case for large spurs exposed in places like the Rheasilvia rim scarp along Matronalia Rupes (Krohn et al. 2014), which have spectral signatures consistent with pure orthopyroxenitic diogenite (Ammannito et al. 2013b; McFadden et al. 2015). Many craters that expose competent material are also found on regions that are thought to be dominated by ejecta from the Rheasilvia impact (Schenk et al. 2012). The presence of blocks in the ejecta of craters that formed within Rheasilvia ejecta is likely due to impact events that encountered large blocks or breccias produced by the Rheasilvia impact event rather than bedrock. The fact that competent material is found within Rheasilvia ejecta also supports the idea that the features mapped here are largely indicative of impacts that occurred within the megaregolith and none require the presence of bedrock.

The regions described above are in contrast to the large equatorial area of low-albedo (Reddy et al. 2012a; Li et al. 2013) from ~100° to 240°E, which contains very few craters <12 km in diameter with boulders (Fig. 2) and fewer craters with resistant material in their walls (Fig. 4) aside from those that overlie the Rheasilvia rim scarp. The regolith is likely substantially thicker here, commonly extending to depths >1 km. This interpretation is supported by evidence that craters smaller than ~400 m are preferentially degraded (Fig. 6A) as compared to those found within Rheasilvia, consistent with their formation in a thicker regolith. A similar conclusion was reached by Vincent et al. (2014) on the basis of crater depth-to-diameter (d/D) ratios. They found craters to be, on average, shallower in the northern hemisphere with d/D ratios of 0.15 ± 0.01, compared to d/D ratios of 0.19 ± 0.01 in the southern impact basins, likely due to a difference in the surface properties.

The region we interpret to have thicker regolith is host to a large fraction of the craters that have low-reflectance material in their walls and ejecta (McCord et al. 2012), including spectacular layering of low-reflectance material exposed in the wall of Marcia crater <1 km below the rim (McCord et al. 2012; Jaumann et al. 2014; Williams et al. 2014). A regolith depth often >1 km in this area supports the idea that the complicated stratigraphy of high- and low-reflectance material in the region is at least in part due to layering within the regolith from impact mixing of exogenic carbonaceous chondrite material.

Surface age on airless planetary bodies generally correlates with crater density, excluding the density of small (less than ~300 m) craters, as previously mentioned. On Vesta, it has been hypothesized that surface age also correlates with decreasing albedo and increasing hydrogen (H) abundance, both of which may be due to carbonaceous chondrite in-mixing over time (De Sanctis et al. 2012; McCord et al. 2012; Prettyman et al. 2012). Surface age on Vesta also likely corresponds to lithologic composition. Recall that basaltic eucrites formed the initial igneous surface on Vesta and orthopyroxenitic diogenites and cumulate eucrites formed as deeper seated layers or plutons. With increased impact gardening over time, the basaltic eucrite surface composition becomes diluted by admixture of orthopyroxenitic diogenite and cumulate eucrite, sampled at depth via impact. Thus, regions that have a high fraction of basaltic eucrite have likely experienced a lower degree of resurfacing.

Areas depleted in blocky craters and small craters (relatively thick regolith) appear to correspond, broadly, to areas that consistently have all the vestan characteristics that signify older surface age. The region where we see few blocky craters (~100–240°E) is identified as (1) having low-albedo (Figs. 2A and 4A), (2) being H-rich (Fig. 8B), (3) containing the largest contiguous occurrence of highly cratered terrain (Fig. 8C), and (4) being basaltic eucrite-rich by Dawn's three instruments (GRaND: [Lawrence et al. 2013; Peplowski et al. 2013; Prettyman et al. 2013; Yamashita et al. 2013]; FC: [Thangjam et al. 2013]; VIR: [Fig. 8A] [Ammannito et al. 2013b; Frigeri et al. 2015b; Longobardo et al. 2015]). Note that Thangjam et al. (2013) and Ammannito et al. (2013b) refer to the area between ~100 and 240°E as "eucrite-rich," meaning it could be enriched in basaltic eucrite and/or cumulate eucrite. GRaND data, however, can be used to distinguish basaltic eucrite from cumulate eucrite (Yamashita et al. 2013; Beck et al. 2015), and this area has been identified as basaltic eucrite-rich (Lawrence et al. 2013; Peplowski et al. 2013; Prettyman et al. 2013; Yamashita et al. 2013).

Craters that sampled blocky material at depths ≤1 km and craters that expose competent material in their walls (regions with thinner regolith) are generally concentrated in younger portions of the surface. Recall that we see blocky craters over two broad areas: 0–90°E and ~260–360°E.

The first area with thin regolith from 0–90°E (1) is relatively high in reflectance (Fig. 2A), (2) has moderate to low H abundance (Fig. 8B), (3) does not overlap the most highly cratered terrains (Fig. 8C), and (4) does not appear to be basaltic eucrite-rich; all three of the instruments identify this region as orthopyroxenitic diogenite-rich (GRaND: [Lawrence et al. 2013; Peplowski et al. 2013; Prettyman et al. 2013; Yamashita et al. 2013]; FC: [Thangjam et al. 2013]; VIR: [Ammannito et al. 2013b; Longobardo et al. 2015], Fig. 8A). Note that all of these studies report this area as "diogenite-rich." However, based on the meteorite

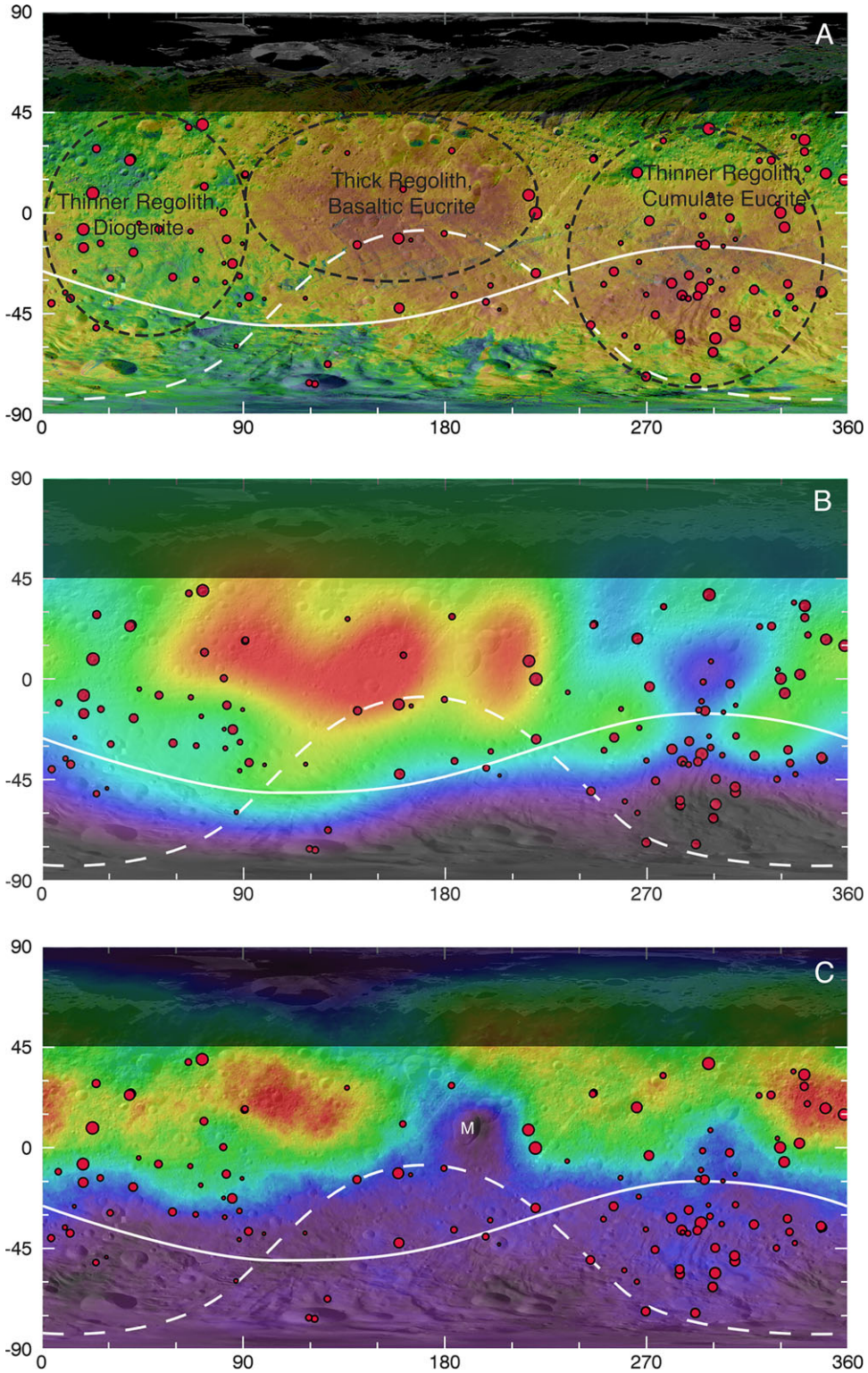

Fig. 8. A) Locations of craters <12 km in diameter that expose blocks (see Fig. 2) on a map of VIR band II center (Ammannito et al. 2013b). Band center data are stretched from 1.93 (blue) to 2.00 (red); longer BII center indicates a more eucritic composition. Regions of thicker and thinner regolith are indicated, along with their inferred compositions. B) Hydrogen content from GRaND range from 0 (black) to 400 μg g^{-1} (red) (Prettyman et al. 2012). C) Crater density map, where values range from 0 (black) to 70 (red) craters per 10^4 km^2 (Marchi et al. 2012); Marcia crater is indicated with an M. Each map is shown overlain on an FC mosaic; approximate Rheasilvia (solid white line) and Veneneia (dashed white line) basin rims are indicated.

data included in those studies, the term "orthopyroxenitic diogenite-rich" is more appropriate (the term "diogenite" includes several meteorite subgroups that were not included in those studies).

The second area with thin regolith from ~260–360°E generally fits characteristics #1–3 denoted above, although a portion of the region does overlap more heavily cratered terrain (Fig. 8C). However, this region of thinner regolith is distinct in criteria #4; it is not enriched in orthopyroxenitic diogenite. This area has been identified as "eucrite-rich" using FC (Thangjam et al. 2013) and VIR (Ammannito et al. 2013b; Frigeri et al. 2015a; Tosi et al. 2015) data, which, again, signifies that it is enriched in basaltic eucrite and/or cumulate eucrite. FC and VIR lithologic maps were created using band one and/or band two (BI and BII, respectively) centers. These are the center wavelength for the ~1 and ~2 μm crystal field absorptions in pyroxene (with possible contributions from olivine at 1 μm), and their center position varies depending on the pyroxene composition (Fe and Ca content) (Hazen et al. 1978; Burns 1993). Cumulate eucrite BI/BII centers overlap basaltic eucrite and basaltic eucrite-rich howardite (e.g., fig. 4 of McSween et al. 2013), and thus, they cannot be resolved in BI/BII center-space. However, based on GRaND Fe and macroscopic thermal neutron absorption cross section data, Yamashita et al. (2013) suggest that a portion of this region is cumulate eucrite-rich, not basaltic eucrite-rich. Further, GRaND fast neutron count data from the ~260–360°E region have moderate to low values (Lawrence et al. 2013), which are consistent with cumulate eucrite, not basaltic eucrite (Beck et al. 2015). Thus, it is probable that this area is enriched in cumulate, not basaltic, eucrite. As such, both regions identified as having relatively thin regolith are in areas where a unit that originally formed at depth (orthopyroxenitic diogenite and cumulate eucrite) is now exposed on the surface.

It is interesting that there is not a 1:1 relationship between regolith depth and surface age as inferred from crater density (Fig. 8C). One area in which the regolith appears to be deep, but the crater density is low, is the region surrounding Marcia crater (~9°N, 190°E). This ~70 km crater resurfaced much of the area surrounding it, leading to a lower crater density in that region, but a thick regolith, where the ejecta contributed to an already substantial fragmental covering. Regions with a high concentration of blocky craters generally correspond to areas with a lower crater density, but do overlap a portion of one of the most heavily cratered terrains (Fig. 8C; 350°E, 20°N).

As the craters that expose blocks are among the most likely to have excavated through mixed regolith to a single compositional unit, we examined VIR data for each blocky crater. A small area on the crater ejecta was defined and VIR BI and BII center data (Ammannito et al. 2013b) were extracted and averaged. The BI and BII centers for the blocky crater ejecta largely overlap the VIR data cloud (Fig. 9). However, some locations do extend into the "pure" orthopyroxenitic diogenite (short BI and BII center wavelengths) and basaltic eucrite (long BI and BII centers) fields.

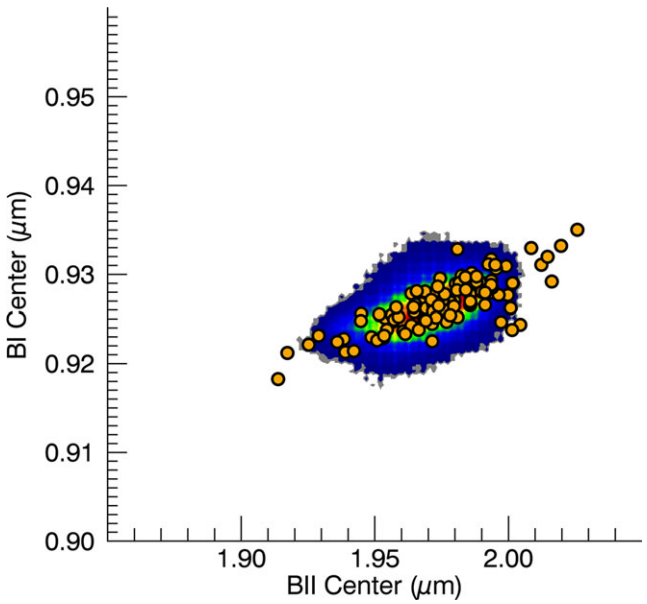

Fig. 9. Band I and II centers from VIR (Ammannito et al. 2013b). The global VIR data are shown as a density plot (low to high density shown as blue to red) and the ejecta of craters that have excavated blocks identified in this study are shown in orange. Most of the ejecta data overlap the global VIR cloud and fall within the howardite field; the shortest band centers are orthopyroxenitic diogenite-like and the longest are eucritic.

We examined the locations (Fig. 10) of craters that are compositional outliers (BII centers <1.95 μm or >2.0 μm, Fig. 9). The orthopyroxenitic diogenite-like craters fall in two groups: those within the Rheasilvia basin or just outside its rim, and a separate group at northern latitudes. Exposures of diogenite near the Rheasilvia basin are consistent with the basin-forming event having excavated this cumulate material from depth, and the craters we examined here have re-exposed it from beneath the regolith. The northern group is unlikely to be related to the southern impact basins. It is well outside the Rheasilvia ejecta blanket (Schenk et al. 2012) and there is a large latitudinal gap where craters that excavated blocks do not expose this material (Fig. 10). We conclude that this group of craters at northern latitudes likely exposes locally

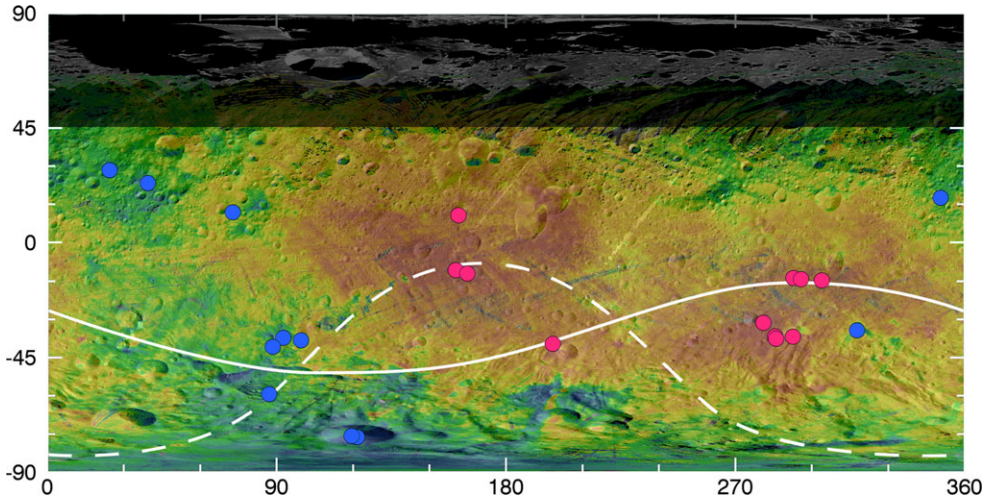

Fig. 10. Locations of craters that expose blocks and have band II centers shorter than 1.95 μm (blue, orthopyroxenitic diogenite) and longer than 2.0 μm (pink, eucritic). The approximate Rheasilvia (solid white line) and Veneneia (dashed white line) rims are shown.

derived material not clearly relatable to any larger impact, thus may be exposed more-or-less in situ. Why this unit, with an orthopyroxenitic diogenite composition (formed as a cumulate at depth), currently resides <1 km from the surface is not clear, although these craters do lie within a relative topographic low (see Fig. 2B).

The craters that expose eucritic material also fall into two groups: one cluster near 180°E longitude and another near 300°E longitude. The first group is within the region of thicker regolith and likely represents small exposures of the original basaltic eucrite surface of Vesta from beneath the regolith. The second group is within an area of thinner regolith that is consistent with cumulate eucrites in the GRaND, VIR, and FC data (see previous discussion). Like the group of the orthopyroxenitic diogenite material near Rheasilvia, the cumulate eucrite-like group is within the Rheasilvia basin or just outside its rim. It is likely that the Rheasilvia basin-forming event excavated the cumulate eucrite material from depth, and the craters we examined here have re-exposed it from beneath the regolith.

The fact that even craters with blocks in their ejecta typically fall within the howardite BI/BII field (Fig. 9) is consistent with relatively rapid mixing of regolith. Craters that we would expect to have exposed diogenite or eucrite material, based on their proximity to nearby exposures, instead often have spectral characteristics of howardites. When examining these craters in FC data, they frequently do not have a well-defined ejecta blanket and have many small, superposed craters. Thus, these craters may have excavated material of a distinct composition, but they have been "weathered" to a more howarditic composition by impact mixing and gardening (Pieters et al. 2012).

We make a first-order comparison of the results presented here to meteorite data by examining the concentrations of basaltic eucrite and orthopyroxenitic diogenite in regolithic howardites. Howardite composition can be quantified by the percent of (basaltic) eucrite material parameter, or "POEM" (Jerome and Goles 1971), where high POEM values indicate basaltic eucrite-rich howardites and low POEM values indicate orthopyroxenitic diogenite-rich howardites. Note, similar comparisons were made by Mittlefehldt (2015). Although POEM oversimplifies the petrologic diversity in the HED clan (reviewed by Beck et al. 2015), it provides a good first-order approach to determining lithologic abundances in howardites. The mean POEM of regolithic howardites is not significantly different from the mean POEM of the rest of the howardite group (Fig. 11). However, it is clear that none of the regolithic howardites have a significant orthopyroxenitic diogenite component, whereas some nonregolithic howardites do contain a majority of orthopyroxenitic diogenite material (Fig. 11). The meteorite data suggest that basaltic eucrite comprises a higher volume percent of the regolith on Vesta than orthopyroxenitic diogenite. The large component of basaltic eucrite in howardite samples generally supports our observations on Vesta. If it is assumed that the deep, basaltic eucrite-rich regolith in the equatorial region from ~100–240°E covers approximately the same surface area as relatively thin regolith in the 0–90°E and ~260–360°E regions, then the basaltic eucrite-rich region

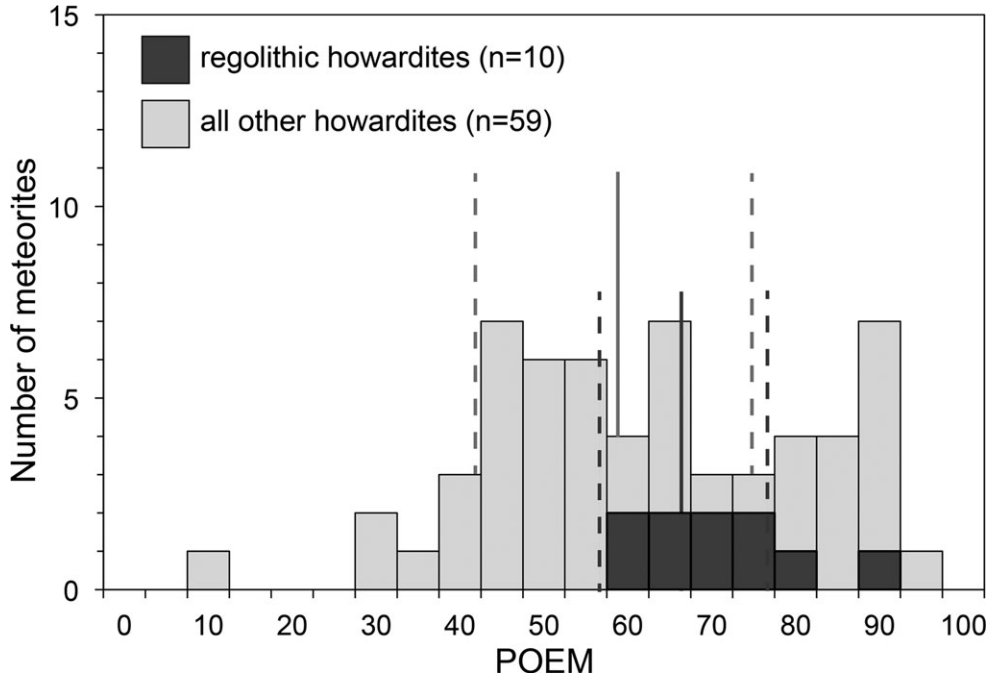

Fig. 11. Percent of basaltic eucrite material (POEM) in regolithic howardites versus the rest of the howardite group. Solid lines are means (regolithic = 68, other = 61), dashed lines are 1σ (regolithic = 10, other = 17). Howardite POEM values are from Beck et al. (2015). Regolithic howardites are those that are gas-rich (Cartwright et al. 2013) and/or have a high petrologic regolithic index (Mittlefehldt et al. 2013).

would comprise a majority of the total volume percent of regolith of Vesta.

CONCLUSIONS

We carried out an assessment of the regolith on Vesta from high-resolution observations of blocks, crater walls, and small crater populations, and compositional inferences from Dawn's VIR, GRaND, and FC instruments as well as regolithic howardites. Our findings lead to the following conclusions.

The distribution of craters <12 km in diameter that have excavated blocky material (excavation depth <1 km) suggests the regolith on Vesta extends to depths greater than 1 km in some places.

The deepest regolith on Vesta is found at equatorial latitudes from ~100–240°E. This region corresponds to the largest contiguous area of heavily cratered terrain on Vesta, with a basaltic eucrite composition that is low in albedo and enriched in carbonaceous chondrite material. The thick regolith is consistent with this region being the battered remains of the original surface of Vesta and recording a history of accumulation of exogenic debris.

Thinner regolith is found in the Rheasilvia basin and at longitudes from ~0–90°E and ~260–360°E. Differences in regolith properties between the portions of Rheasilvia that did and did not overlap the Veneneia basin suggest that areas where the two basins intersect may be substantially more fractured and fragmented. Craters that excavate through the regolith in the Rheasilvia basin and from 0–90°E are more diogenitic; from ~260–360°E they expose cumulate eucrite material.

Craters that have excavated blocks most commonly formed in howarditic material. Many of these craters may only excavate material from within the regolith or megaregolith, although these observations are also consistent with gardening ("weathering") of ejecta toward howardite compositions.

Acknowledgments—We thank W. Fa, L. McFadden, and an anonymous reviewer for helpful suggestions. We gratefully acknowledge the support of the Dawn Science, Instrument and Operations Teams. BWD was supported by the Dawn at Vesta Participating Scientist program through NASA Grant NNX11AC28G.

Editorial Handling—Dr. Gretchen Benedix

REFERENCES

Ammannito E., De Sanctis M. C., Palomba E., Longobardo A., Mittlefehldt D. W., McSween H. Y., Marchi S., Capria M. T., Capaccioni F., Frigeri A., Pieters C. M.,

Ruesch O., Tosi F., Zambon F., Carraro F., Fonte S., Hiesinger H., Magni G., McFadden L. A., Raymond C. A., Russell C. T., and Sunshine J. M. 2013a. Olivine in an unexpected location on Vesta's surface. *Nature* 504:122–125. doi:10.1038/nature12665.

Ammannito E., De Sanctis M. C., Capaccioni F., Teresa Capria M., Carraro F., Combe J.-P., Fonte S., Frigeri A., Joy S. P., Longobardo A., Magni G., Marchi S., McCord T. B., McFadden L. A., McSween H. Y., Palomba E., Pieters C. M., Polanskey C. A., Raymond C. A., Sunshine J. M., Tosi F., Zambon F., and Russell C. T. 2013b. Vestan lithologies mapped by the visual and infrared spectrometer on Dawn. *Meteoritics & Planetary Science* 48:2185–2198. doi:10.1111/maps.12192.

Basilevsky A. T., Head J. W., and Horz F. 2013. Survival times of meter-sized boulders on the surface of the Moon. *Planetary and Space Science* 89:118–126. doi:10.1016/j.pss.2013.07.011.

Basilevsky A. T., Head J. W., Horz F., and Ramsley K. 2014. Survival time of meter-sized rock boulders on the surface of asteroid Itokawa (abstract #1688). 45th Lunar and Planetary Science Conference. CD-ROM.

Beck A. W., Lawrence D. J., Peplowski P. N., Prettyman T. H., McCoy T. J., McSween H. Y., Toplis M. J., and Yamashita N. 2015. Using HED meteorites to interpret neutron and gamma ray data from asteroid 4 Vesta. *Meteoritics & Planetary Science* 50:1311–1337. doi:10.1111/maps.12467.

Binzel R. P. and Xu S. 1993. Chips off of asteroid 4 Vesta: Evidence for the parent body of basaltic achondrite meteorites. *Science* 260:186–191.

Blewett D. T., Denevi B. W., Le Corre L., Reddy V., Schröder S. E., Pieters C. M., Tosi F., Zambon F., De Sanctis M. C., Ammannito E., Roatsch T., Raymond C. A., and Russell C. T. 2016. Optical space weathering on Vesta: Radiative-transfer models and Dawn observations. *Icarus* 265:161–174. doi:10.1016/j.icarus.2015.10.012.

Burbine T. H., Buchanan P. C., Binzel R. P., Bus S. J., Hiroi T., Hinrichs J. L., Meibom A., and McCoy T. J. 2001. Vesta, vestoids, and the howardite, eucrite, diogenite group: Relationships and the origin of spectral differences. *Meteoritics & Planetary Science* 36:761–781. doi:10.1111/j.1945-5100.2001.tb01915.x.

Burns R. G. 1993. *Mineralogical applications of crystal field theory*. Cambridge, UK: Cambridge University Press.

Capria M. T., Tosi F., De Sanctis M. C., Capaccioni F., Ammannito E., Frigeri A., Zambon F., Fonte S., Palomba E., Turrini D., Titus T. N., Schröder S. E., Toplis M., Li J.-Y., Combe J.-P., Raymond C. A., and Russell C. T. 2014. Vesta surface thermal properties map. *Geophysical Research Letters*, 41:2013GL059026. doi:10.1002/2013GL059026.

Carr M. H., Kirk R. L., McEwen A. S., Veverka J., Thomas P., Head J. W., and Murchie S. 1994. The geology of Gaspra. *Icarus* 107:67–71.

Cartwright J. A., Ott U., Mittlefehldt D. W., Herrin J. S., Herrmann S., Mertzman S. A., Mertzman K. R., Peng Z. X., and Quinn J. E. 2013. The quest for regolithic howardites. Part 1: Two trends uncovered using noble gases. *Geochimica et Cosmochimica Acta* 105:395–421. doi:10.1016/j.gca.2012.11.047.

Cintala M. J. and McBride K. M. 1995. Block distribution on the lunar surface: A comparison between measurements obtained from surface and orbital Photography. *NASA Technical Memo 104804*. 41 p.

Cintala M. J., Head J. W., and Veverka J. 1978. Characteristics of the cratering process on small satellites and asteroids. Proceedings, 9th Lunar and Planetary Science Conference. pp. 3803–3830.

Clark B. E., Hapke B., Pieters C., and Britt D. 2002. Asteroid space weathering and regolith evolution. In *Asteroids III*, edited by Bottke W. F., Cellino A., Paolicchi P., and Binzel R. P. Tucson, Arizona: The Univeristy of Arizona Press. pp. 585–599.

Combe J.-P., McCord T. B., McFadden L. A., Ieva S., Tosi F., Longobardo A., Frigeri A., Sanctis M. C. D., Ammannito E., Ruesch O., Palomba E., Raymond C. A., and Russell C. T. 2015. Composition of the northern regions of Vesta analyzed by the Dawn mission. *Icarus* 259:53–71. doi:10.1016/j.icarus.2015.04.026.

Crater Analysis Techniques Working Group. 1979. Standard techniques for presentation and analysis of crater size-frequency data. *Icarus* 37:467–474.

Croft S. K. 1981. Relationships between the apparent crater, transient crater, and excavation cavity of a simple crater. In *Workshop on Apollo 16*, edited by James O. B. and Hörz F. Houston, Texas: Lunar and Planetary Institute. 40 p.

De Sanctis M. C., Combe J.-P., Ammannito E., Palomba E., Longobardo A., McCord T. B., Marchi S., Capaccioni F., Capria M. T., Mittlefehldt D. W., Pieters C. M., Sunshine J., Tosi F., Zambon F., Carraro F., Fonte S., Frigeri A., Magni G., Raymond C. A., Russell C. T., and Turrini D. 2012. Detection of widespread hydrated materials on Vesta by the VIR imaging spectrometer on board the Dawn Mission. *The Astrophysical Journal* 758:L36. doi:10.1088/2041-8205/758/2/L36.

Delbo M., Libourel G., Wilkerson J., Murdoch N., Michel P., Ramesh K. T., Ganino C., Verati C., and Marchi S. 2014. Thermal fatigue as the origin of regolith on small asteroids. *Nature* 508:233–236.

Fa W., Liu T., Zhu M.-H., and Haruyama J. 2014. Regolith thickness over Sinus Iridum: Results from morphology and size-frequency distribution of small impact craters. *Journal of Geophysical Research: Planets* 119:1914–1935. doi:10.1002/2013JE004604.

Frigeri A., De Sanctis M. C., Ammannito E., Buczkowski D., Combe J. P., Tosi F., Zambon F., Rocchini D., Jaumann R., Raymond C. A., and Russell C. T. 2015a. Mineralogic mapping of the Av-9 Numisia quadrangle of Vesta. *Icarus* 259:116–128. doi:10.1016/j.icarus.2015.07.029.

Frigeri A., De Sanctis M. C., Ammannito E., Tosi F., Longobardo A., Zambon F., McCord T., Combe J. P., Jaumann R., Raymond C. A., and Russell C. T. 2015b. The spectral parameter maps of Vesta from VIR data. *Icarus* 259:10–20. doi:10.1016/j.icarus.2015.06.027.

Gaskell R. W. 2012. SPC shape and topography of Vesta from Dawn imaging data. *American Astronomical Society. DPS meeting #44*, 209.03.

Gaskell R. W., Barnouin-Jha O. S., Scheeres D. J., Konopliv A. S., Mukai T., Abe S., Saito J., Ishiguro M., Kubota T., Hashimoto T., Kawaguchi J., Yoshikawa M., Shirakawa K., Kominato T., Hirata N., and Demura H. 2008. Characterizing and navigating small bodies with imaging data. *Meteoritics & Planetary Science* 43:1049–1061.

Hansen T. P. 1970. *Guide to lunar orbiter photographs*. NASA SP-242. Washington, D.C.: Scientific and Technical Information Office, National Aeronautics and Space Administration.

Hapke B. 2001. Space weathering from Mercury to the asteroid belt. *Journal of Geophysical Research* 106:10,039–10,073.

Hartmann W. K. 1973. Ancient lunar mega-regolith and subsurface structure. *Icarus* 18:634–636.

Haruyama J., Matsunaga T., Ohtake M., Morota T., Honda C., Yokota Y., Torii M., Ogawa Y., and the LISM Working Group. 2008. Global lunar-surface mapping experiment using the Lunar Imager/Spectrometer on SELENE. *Earth, Planets and Space* 60:243–255.

Hazen R. M., Bell P. M., and Mao H. K. 1978. Effects of compositional variation on absorption spectra of lunar pyroxenes. Proceedings, 9th Lunar and Planetary Science Conference. pp. 2919–2934.

Helfenstein P., Veverka J., Thomas P. C., Simonelli D. P., Lee P., Klaasen K., Johnson T. V., Breneman H., Head J. W., Murchie S., Fanale F., Robinson M., Clark B., Granahan J., Garbeil H., McEwen A. S., Kirk R. L., Davies M., Neukum G., Mottola S., Wagner R., Belton M., Chapman C., and Pilcher C. 1994. Galileo photometry of Asteroid 951 Gaspra. *Icarus* 107:37–60.

Helfenstein P., Veverka J., Thomas P. C., Simonelli D. P., Klaasen K., Johnson T. V., Fanale F., Granahan J., McEwen A. S., Belton M., and Chapman C. 1996. Galileo photometry of Asteroid 243 Ida. *Icarus* 120:48–65.

Hirata N., Barnouin-Jha O. S., Honda C., Nakamura R., Miyamoto H., Sasaki S., Demura H., Nakamura A. M., Michikami T., Gaskell R. W., and Saito J. 2009. A survey of possible impact structures on 25143 Itokawa. *Icarus* 200:486–502. doi:10.1016/j.icarus.2008.10.027.

Hiroi T., Pieters C. M., and Takeda H. 1994. Grain size of the surface regolith of asteroid 4 Vesta estimated from its reflectance spectrum in comparison with HED meteorites. *Meteoritics* 29:394–396.

Hörz F., Schneider E., Gault D. E., Hartung J. B., and Brownlee D. E. 1975. Catastrophic rupture of lunar rocks: A Monte Carlo simulation. *The Moon* 13:235–258.

Isbell C., Gaddis L., Garcia P., Hare T., and Bailen M. 2014. Kaguya Terrain Camera Mosaics (abstract #2268). 45th Lunar and Planetary Science Conference. CD-ROM.

Jaumann R., Williams D. A., Buczkowski D. L., Yingst R. A., Preusker F., Hiesinger H., Schmedemann N., Kneissl T., Vincent J. B., Blewett D. T., Buratti B. J., Carsenty U., Denevi B. W., De Sanctis M. C., Garry W. B., Keller H. U., Kersten E., Krohn K., Li J.-Y., Marchi S., Matz K. D., McCord T. B., McSween H. Y., Mest S. C., Mittlefehldt D. W., Mottola S., Nathues A., Neukum G., O'Brien D. P., Pieters C. M., Prettyman T. H., Raymond C. A., Roatsch T., Russell C. T., Schenk P., Schmidt B. E., Scholten F., Stephan K., Sykes M. V., Tricarico P., Wagner R., Zuber M. T., and Sierks H. 2012. Vesta's shape and morphology. *Science* 336:687–690. doi:10.1126/science.1219122.

Jaumann R., Nass A., Otto K., Krohn K., Stephan K., McCord T. B., Williams D. A., Raymond C. A., Blewett D. T., Hiesinger H., Yingst R. A., De Sanctis M. C., Palomba E., Roatsch T., Matz K.-D., Preusker F., Scholten F., and Russell C. T. 2014. The geological nature of dark material on Vesta and implications for the subsurface structure. *Icarus* 240:3–19. doi:10.1016/j.icarus.2014.04.035.

Jerome J. Y. and Goles G. G. 1971. A re-examination of relationships among pyroxene-plagioclase achondrites. In *Activation analysis in geochemistry and cosmochemistry*, edited by Brunfelt A. O. and Seinnes E.. Oslo: Universitetsfrolaget. pp. 261–266.

Kahn E. G., Barnouin O. S., Buczkowski D. L., Ernst C. M., Izenberg N. R., Murchie S. L., and Prockter L. M. 2011. A tool for the visualization of small body data (abstract #1618). 42nd Lunar and Planetary Science Conference. CD-ROM.

Krohn K., Jaumann R., Otto K., Hoogenboom T., Wagner R., Buczkowski D. L., Garry B., Williams D. A., Yingst R. A., Scully J., De Sanctis M. C., Kneissl T., Schmedemann N., Kersten E., Stephan K., Matz K.-D., Pieters C. M., Preusker F., Roatsch T., Schenk P., Russell C. T., and Raymond C. A. 2014. Mass movement on Vesta at steep scarps and crater rims. *Icarus* 244:120–132. doi:10.1016/j.icarus.2014.03.013.

Lawrence D. J., Peplowski P. N., Prettyman T. H., Feldman W. C., Bazell D., Mittlefehldt D. W., Reedy R. C., and Yamashita N. 2013. Constraints on Vesta's elemental composition: Fast neutron measurements by Dawn's gamma ray and neutron detector. *Meteoritics & Planetary Science* 48:2271–2288. doi:10.1111/maps.12187.

Li J.-Y., Le Corre L., Schröder S. E., Reddy V., Denevi B. W., Buratti B. J., Mottola S., Hoffmann M., Gutierrez-Marques P., Nathues A., Russell C. T., and Raymond C. A. 2013. Global photometric properties of Asteroid (4) Vesta observed with Dawn Framing Camera. *Icarus* 226:1252–1274. doi:10.1016/j.icarus.2013.08.011.

Longobardo A., Palomba E., De Sanctis M. C., Zinzi A., Scully J. E. C., Capaccioni F., Tosi F., Zambon F., Ammannito E., Combe J.-P., Raymond C. A., and Russell C. T. 2015. Mineralogical and spectral analysis of Vesta's Gegania and Lucaria quadrangles and comparative analysis of their key features. *Icarus* 259:72–90. doi:10.1016/j.icarus.2015.04.031.

Lugmair G. W. and Shukolyukov A. 1998. Early solar system timescales according to 53Mn-53Cr systematics. *Geochimica et Cosmochimica Acta* 62:2863–2886. doi:10.1016/S0016-7037(98)00189-6.

Marchi S., McSween H. Y., O'Brien D. P., Schenk P., Sanctis M. C. D., Gaskell R., Jaumann R., Mottola S., Preusker F., Raymond C. A., Roatsch T., and Russell C. T. 2012. The violent collisional history of Asteroid 4 Vesta. *Science* 336:690–694. doi:10.1126/science.1218757.

Matson D. L., Johnson T. V., and Veeder G. J. 1977. Soil maturity and planetary regoliths—The Moon, Mercury, and the asteroids. 8th Lunar Science Conference. pp. 1001–1011.

McCord T. B., Adams J. B., and Johnson T. V. 1970. Asteroid Vesta: Spectral reflectivity and compositional implications. *Science* 168:1445–1447.

McCord T. B., Li J.-Y., Combe J.-P., McSween H. Y., Jaumann R., Reddy V., Tosi F., Williams D. A., Blewett D. T., Turrini D., Palomba E., Pieters C. M., De Sanctis M. C., Ammannito E., Capria M. T., Le Corre L., Longobardo A., Nathues A., Mittlefehldt D. W., Schröder S. E., Hiesinger H., Beck A. W., Capaccioni F., Carsenty U., Keller H. U., Denevi B. W., Sunshine J. M., Raymond C. A., and Russell C. T. 2012. Dark material on Vesta from the infall of carbonaceous volatile-rich material. *Nature* 491:83–86. doi:10.1038/nature11561.

McFadden L. A., Combe J.-P., Ammannito E., Frigeri A., Stephan K., Longobardo A., Palomba E., Tosi F., Zambon F., Krohn K., De Sanctis M. C., Reddy V., Le Corre L., Nathues A., Pieters C. M., Prettyman T. H.,

Raymond C. A., and Russell C. T. 2015. Vesta's Pinaria region: Original basaltic achondrite material derived from mixing upper and lower crust. *Icarus* 259:150–161. doi:10.1016/j.icarus.2015.07.003.

McSween H. Y., Mittlefehldt D. W., Beck A. W., Mayne R. G., and McCoy T. J. 2011. HED meteorites and their relationship to the geology of Vesta and the Dawn Mission. *Space Science Reviews* 163:141–174. doi:10.1007/s11214-010-9637-z.

McSween H. Y., Binzel R. P., De Sanctis M. C., Ammannito E., Prettyman T. H., Beck A. W., Reddy V., Le Corre L., Gaffey M. J., McCord T. B., Raymond C. A., and Russell C. T. 2013. Dawn; the Vesta–HED connection; and the geologic context for eucrites, diogenites, and howardites. *Meteoritics & Planetary Science* 48:2090–2104. doi:10.1111/maps.12108.

Melosh H. J. 1989. *Impact cratering: A geologic process*. New York: Oxford University Press.

Mittlefehldt D. W. 2015. Asteroid (4) Vesta: I. The howardite-eucrite-diogenite (HED) clan of meteorites. *Chemie der Erde—Geochemistry* 75:155–183. doi:10.1016/j.chemer.2014.08.002.

Mittlefehldt D. W., Herrin J. S., Quinn J. E., Mertzman S. A., Cartwright J. A., Mertzman K. R., and Peng Z. X. 2013. Composition and petrology of HED polymict breccias: The regolith of (4) Vesta. *Meteoritics & Planetary Science* 48:2105–2134. doi:10.1111/maps.12182.

Murchie S., Robinson M., Clark B., Li H., Thomas P., Joseph J., Bussey B., Domingue D., Veverka J., Izenberg N., and Chapman C. 2002. Color variations on Eros from NEAR multispectral imaging. *Icarus* 155:145–168. doi:10.1006/icar.2001.6756.

Oberbeck V. R. and Quaide W. L. 1968. Genetic implications of lunar regolith thickness variations. *Icarus* 9:446–465.

Oberbeck V. R., Quaide W. L., Mahan M., and Paulson J. 1973. Monte Carlo calculations of lunar regolith thickness distributions. *Icarus* 19:87–107.

O'Keefe J. D. and Ahrens T. J. 1987. Impact crater maximum depth of penetration and excavation. Proceedings, 18th Lunar and Planetary Science Conference. p. 744.

Palomba E., Longobardo A., De Sanctis M. C., Zinzi A., Ammannito E., Marchi S., Tosi F., Zambon F., Capria M. T., Russell C. T., Raymond C. A., and Cloutis E. A. 2015. Detection of new olivine-rich locations on Vesta. *Icarus* 258:120–134. doi:10.1016/j.icarus.2015.06.011.

Peplowski P. N., Lawrence D. J., Prettyman T. H., Yamashita N., Bazell D., Feldman W. C., Le Corre L., McCoy T. J., Reddy V., Reedy R. C., Russell C. T., and Toplis M. J. 2013. Compositional variability on the surface of 4 Vesta revealed through GRaND measurements of high-energy gamma rays. *Meteoritics & Planetary Science* 48:2252–2270. doi:10.1111/maps.12176.

Pieters C. M., Fischer E. M., Rode O., and Basu A. 1993. Optical effects of space weathering: The role of the finest fraction. *Journal of Geophysical Research* 98:20,817–20,824.

Pieters C. M., Taylor L., Noble S., Keller L., Hapke B., Morris R., Allen C., McKay D., and Wentworth S. 2000. Space weathering on airless bodies: Resolving a mystery with lunar samples. *Meteoritics & Planetary Science* 35:1101–1107.

Pieters C. M., Ammannito E., Blewett D. T., Denevi B. W., De Sanctis M. C., Gaffey M. J., Le Corre L., Li J.-Y., Marchi S., McCord T. B., McFadden L. A., Mittlefehldt D. W., Nathues A., Palmer E., Reddy V., Raymond C. A., and Russell C. T. 2012. Distinctive space weathering on Vesta from regolith mixing processes. *Nature* 491:79–82. doi:10.1038/nature11534.

Prettyman T. H., Mittlefehldt D. W., Yamashita N., Lawrence D. J., Beck A. W., Feldman W. C., McCoy T. J., McSween H. Y., Toplis M. J., Titus T. N., Tricarico P., Reedy R. C., Hendricks J. S., Forni O., Le Corre L., Li J.-Y., Mizzon H., Reddy V., Raymond C. A., and Russell C. T. 2012. Elemental mapping by Dawn reveals exogenic H in Vesta's regolith. *Science* 338:242–246. doi:10.1126/science.1225354.

Prettyman T. H., Mittlefehldt D. W., Yamashita N., Beck A. W., Feldman W. C., Hendricks J. S., Lawrence D. J., McCoy T. J., McSween H. Y., Peplowski P. N., Reedy R. C., Toplis M. J., Le Corre L., Mizzon H., Reddy V., Titus T. N., Raymond C. A., and Russell C. T. 2013. Neutron absorption constraints on the composition of 4 Vesta. *Meteoritics & Planetary Science* 48:2211–2236. doi:10.1111/maps.12244.

Quaide W. L. and Oberbeck V. R. 1968. Thickness determinations of the lunar surface layer from lunar impact craters. *Journal of Geophysical Research* 73:5247–5270.

Reddy V., Le Corre L., O'Brien D. P., Nathues A., Cloutis E. A., Durda D. D., Bottke W. F., Bhatt M. U., Nesvorný D., Buczkowski D., Scully J. E. C., Palmer E. M., Sierks H., Mann P. J., Becker K. J., Beck A. W., Mittlefehldt D., Li J.-Y., Gaskell R., Russell C. T., Gaffey M. J., McSween H. Y., McCord T. B., Combe J.-P., and Blewett D. 2012a. Delivery of dark material to Vesta via carbonaceous chondritic impacts. *Icarus* 221:544–559. doi:10.1016/j.icarus.2012.08.011.

Reddy V., Nathues A., Le Corre L., Sierks H., Li J.-Y., Gaskell R., McCoy T., Beck A. W., Schröder S. E., Pieters C. M., Becker K. J., Buratti B. J., Denevi B., Blewett D. T., Christensen U., Gaffey M. J., Gutierrez-Marques P., Hicks M., Keller H. U., Maue T., Mottola S., McFadden L. A., McSween H. Y., Mittlefehldt D., O'Brien D. P., Raymond C., and Russell C. 2012b. Color and albedo heterogeneity of Vesta from Dawn. *Science* 336:700–704. doi:10.1126/science.1219088.

Rennilson J. J., Dragg J. L., Morris E. C., Shoemaker E. M., and Turkevich A. 1966. Lunar surface topography. In *Surveyor I mission report, part II: Scientific data and results, NASA-JPL Technical Report 32-1023*. pp. 7–44.

Richardson J. E., Melosh H. J., and Greenberg R. 2004. Impact-induced seismic activity on asteroid 433 Eros: A surface modification process. *Science* 306:1526–1529. doi:10.1126/science.1104731.

Richardson J. E. Jr., Melosh H. J., Greenberg R. J., and O'Brien D. P. 2005. The global effects of impact-induced seismic activity on fractured asteroid surface morphology. *Icarus* 179:325–349. doi:10.1016/j.icarus.2005.07.005.

Roatsch T., Kersten E., Matz K.-D., Preusker F., Scholten F., Jaumann R., Raymond C. A., and Russell C. T. 2012. High resolution Vesta High Altitude Mapping Orbit (HAMO) Atlas derived from Dawn Framing Camera images. *Planetary and Space Science* 73:283–286. doi:10.1016/j.pss.2012.08.021.

Robinson M. S., Thomas P. C., Veverka J., Murchie S. L., and Wilcox B. B. 2002. The geology of 433 Eros. *Meteoritics & Planetary Science* 37:1651–1684.

Ruesch O., Hiesinger H., Blewett D. T., Williams D. A., Buczkowski D., Scully J., Yingst R. A., Roatsch T.,

Preusker F., Jaumann R., Russell C. T., and Raymond C. A. 2014a. Geologic map of the northern hemisphere of Vesta based on Dawn Framing Camera (FC) images. *Icarus* 244:41–59. doi:10.1016/j.icarus.2014.01.035.

Ruesch O., Hiesinger H., De Sanctis M. C., Ammannito E., Palomba E., Longobardo A., Zambon F., Tosi F., Capria M. T., Capaccioni F., Frigeri A., Fonte S., Magni G., Raymond C. A., and Russell C. T. 2014b. Detections and geologic context of local enrichments in olivine on Vesta with VIR/Dawn data. *Journal of Geophysical Research: Planets*, 119:2014JE004625. doi:10.1002/2014JE004625.

Russell C. T., Raymond C. A., Coradini A., McSween H. Y., Zuber M. T., Nathues A., Sanctis M. C. D., Jaumann R., Konopliv A. S., Preusker F., Asmar S. W., Park R. S., Gaskell R., Keller H. U., Mottola S., Roatsch T., Scully J. E. C., Smith D. E., Tricarico P., Toplis M. J., Christensen U. R., Feldman W. C., Lawrence D. J., McCoy T. J., Prettyman T. H., Reedy R. C., Sykes M. E., and Titus T. N. 2012. Dawn at Vesta: Testing the protoplanetary paradigm. *Science* 336:684–686. doi:10.1126/science.1219381.

Russell C. T., Raymond C. A., Jaumann R., McSween H. Y., De Sanctis M. C., Nathues A., Prettyman T. H., Ammannito E., Reddy V., Preusker F., O'Brien D. P., Marchi S., Denevi B. W., Buczkowski D. L., Pieters C. M., McCord T. B., Li J.-Y., Mittlefehldt D. W., Combe J.-P., Williams D. A., Hiesinger H., Yingst R. A., Polanskey C. A., and Joy S. P. 2013. Dawn completes its mission at 4 Vesta. *Meteoritics & Planetary Science* 48:2076–2089. doi: 10.1111/maps.12091.

Saito J., Miyamoto H., Nakamura R., Ishiguro M., Michikami T., Nakamura A. M., Demura H., Sasaki S., Hirata N., Honda C., Yamamoto A., Yokota Y., Fuse T., Yoshida F., Tholen D. J., Gaskell R. W., Hashimoto T., Kubota T., Higuchi Y., Nakamura T., Smith P., Hiraoka K., Honda T., Kobayashi S., Furuya M., Matsumoto N., Nemoto E., Yukishita A., Kitazato K., Dermawan B., Sogame A., Terazono J., Shinohara C., and Akiyama H. 2006. Detailed images of asteroid 25143 Itokawa from Hayabusa. *Science* 312:1341–1344. doi:10.1126/science.1125722.

Schenk P., O'Brien D. P., Marchi S., Gaskell R., Preusker F., Roatsch T., Jaumann R., Buczkowski D., McCord T., McSween H. Y., Williams D., Yingst A., Raymond C., and Russell C. 2012. The geologically recent giant impact basins at Vesta's South Pole. *Science* 336:694–697. doi:10.1126/science.1223272.

Schmedemann N., Kneissl T., Ivanov B. A., Michael G. G., Wagner R. J., Neukum G., Ruesch O., Hiesinger H., Krohn K., Roatsch T., Preusker F., Sierks H., Jaumann R., Reddy V., Nathues A., Walter S. H. G., Neesemann A., Raymond C. A., and Russell C. T. 2014. The cratering record, chronology and surface ages of (4) Vesta in comparison to smaller asteroids and the ages of HED meteorites. *Planetary and Space Science* 103:104–130. doi:10.1016/j.pss.2014.04.004.

Schröder S. E., Mottola S., Keller H. U., Raymond C. A., and Russell C. T. 2013. Resolved photometry of Vesta reveals physical properties of crater regolith. *Planetary and Space Science* 85:198–213. doi:10.1016/j.pss.2013.06.009.

Scully J. E. C., Russell C. T., Yin A., Jaumann R., Carey E., Castillo-Rogez J., McSween H. Y., Raymond C. A., Reddy V., and Le Corre L. 2015. Geomorphological evidence for transient water flow on Vesta. *Earth and Planetary Science Letters* 411:151–163. doi:10.1016/j.epsl.2014.12.004.

Shoemaker E. M. and Morris E. C. 1970. Geology: Physics of fragmental debris. *Icarus* 12:188–212.

Shoemaker E. M., Batson R. M., Holt H. E., Morris E. C., Rennilson J. J., and Whitaker E. A. 1969. Observations of the lunar regolith and the Earth from the television camera on Surveyor 7. *Journal of Geophysical Research* 74:6081–6119.

Sierks H., Lamy P., Barbieri C., Koschny D., Rickman H., Rodrigo R., A'Hearn M. F., Angrilli F., Barucci M. A., Bertaux J.-L., Bertini I., Besse S., Carry B., Cremonese G., Da Deppo V., Davidsson B., Debei S., De Cecco M., De Leon J., Ferri F., Fornasier S., Fulle M., Hviid S. F., Gaskell R. W., Groussin O., Gutierrez P., Ip W., Jorda L., Kaasalainen M., Keller H. U., Knollenberg J., Kramm R., Kuhrt E., Kuppers M., Lara L., Lazzarin M., Leyrat C., Moreno J. J. L., Magrin S., Marchi S., Marzari F., Massironi M., Michalik H., Moissl R., Naletto G., Preusker F., Sabau L., Sabolo W., Scholten F., Snodgrass C., Thomas N., Tubiana C., Vernazza P., Vincent J.-B., Wenzel K.-P., Andert T., Patzold M., and Weiss B. P. 2011a. Images of asteroid 21 Lutetia: A remnant planetesimal from the early solar system. *Science* 334:487–490. doi:10.1126/science.1207325.

Sierks H., Keller H. U., Jaumann R., Michalik H., Behnke T., Bubenhagen F., Büttner I., Carsenty U., Christensen U., Enge R., Fiethe B., Gutiérrez Marqués P., Hartwig H., Krüger H., Kühne W., Maue T., Mottola S., Nathues A., Reiche K.-U., Richards M. L., Roatsch T., Schröder S. E., Szemerey I., and Tschentscher M. 2011b. The Dawn Framing Camera. *Space Science Reviews* 163:263–327.

Soderblom L. A. 1970. A model for small-impact erosion applied to the lunar surface. *Journal of Geophysical Research* 75:2655–2661.

Sullivan R. 1992. Three-dimensional stability back-analysis of small Martian avalanche chutes. Proceedings, 23rd Lunar and Planetary Science Conference. pp. 1385–1386.

Thangjam G., Reddy V., Le Corre L., Nathues A., Sierks H., Hiesinger H., Li J.-Y., Sanchez J. A., Russell C. T., Gaskell R., and Raymond C. 2013. Lithologic mapping of HED terrains on Vesta using Dawn Framing Camera color data. *Meteoritics & Planetary Science* 48:2199–2210. doi:10.1111/maps.12132.

Thomas P. C. and Robinson M. S. 2005. Seismic resurfacing by a single impact on the asteroid 433 Eros. *Nature* 436:366–369.

Thomas P., Joseph J., Carcich B., Veverka J., Clark B. E., Bell J. F. I., Byrd A. W., Chomko R., Robinson M., Murchie S., Prockter L., Cheng A., Izenberg N., Malin M., Chapman C., McFadden L. A., Kirk R., Gaffey M., and Lucey P. G. 2002. Eros: Shape, topography, and slope processes. *Icarus* 155:18–37. doi:10.1006/icar.2001.6755.

Tosi F., Frigeri A., Combe J.-P., Zambon F., De Sanctis M. C., Ammannito E., Longobardo A., Hoffmann M., Nathues A., Garry W. B., Blewett D. T., Pieters C. M., Palomba E., Stephan K., McFadden L. A., McSween H. Y., Russell C. T., and Raymond C. A. 2015. Mineralogical analysis of the Oppia quadrangle of asteroid (4) Vesta: Evidence for occurrence of moderate-reflectance hydrated minerals. *Icarus* 259:129–149. doi:10.1016/j.icarus.2015.05.018.

Trask N. J. and Rowan L. C. 1967. Lunar Orbiter photographs: Some fundamental observations. *Science* 158:1529–1535.

Trinquier A., Birck J.-L., Allègre C. J., Göpel C., and Ulfbeck D. 2008. 53Mn–53Cr systematics of the early solar system revisited. *Geochimica et Cosmochimica Acta* 72:5146–5163. doi:10.1016/j.gca.2008.03.023.

Veverka J., Thomas P. C., Robinson M., Murchie S., Chapman C., Bell M., Harch A., Merline W. J., Bell J. F., Bussey B., Carcich B., Cheng A., Clark B., Domingue D., Dunham D., Farquhar R., Gaffey M. J., Hawkins E., Izenberg N., Joseph J., Kirk R., Li H., Lucey P., Malin M., McFadden L., Miller J. K., Owen W. M., Peterson C., Prockter L., Warren J., Wellnitz D., Williams B. G., and Yeomans D. K. 2001. Imaging of small-scale features on 433 Eros from NEAR: Evidence for a complex regolith. *Science* 292:484–488. doi:10.1126/science.1058651.

Vincent J.-B., Schenk P., Nathues A., Sierks H., Hoffmann M., Gaskell R. W., Marchi S., O'Brien D. P., Sykes M., Russell C. T., Fulchignoni M., Kellerg H. U., Raymond C., Palmer E., and Preusker F. 2014. Crater depth-to-diameter distribution and surface properties of (4) vesta. *Planetary and Space Science* 103: 57–65. doi:10.1016/j.pss.2013.09.003.

Weisberg M. K., McCoy T. J., and Krot A. N. 2006. Systematics and evaluation of meteorite classification. In *Meteorites and the early solar system II*, edited by Lauretta D. S. and McSween H. Y. Tucson, Arizona: The University of Arizona Press. pp. 19–52.

Wilcox B. B., Robinson M. S., Thomas P. C., and Hawke B. R. 2005. Constraints on the depth and variability of the lunar regolith. *Meteoritics & Planetary Science* 40:695–710.

Williams D. A., O'Brien D. P., Schenk P. M., Denevi B. W., Carsenty U., Marchi S., Scully J. E. C., Jaumann R., De Sanctis M. C., Palomba E., Ammannito E., Longobardo A., Magni G., Frigeri A., Russell C. T., Raymond C. A., and Davison T. M. 2013. Lobate and flow-like features on asteroid Vesta. *Planetary and Space Science* 103:24–35. doi:10.1016/j.pss.2013.06.017.

Williams D. A., Denevi B. W., Mittlefehldt D. W., Mest S. C., Schenk P. M., Yingst R. A., Buczkowski D. L., Scully J. E. C., Garry W. B., McCord T. B., Combe J.-P., Jaumann R., Pieters C. M., Nathues A., Le Corre L., Hoffmann M., Reddy V., Schäfer M., Roatsch T., Preusker F., Marchi S., Kneissl T., Schmedemann N., Neukum G., Hiesinger H., De Sanctis M. C., Ammannito E., Frigeri A., Prettyman T. H., Russell C. T., and Raymond C. A. 2014. The geology of the Marcia quadrangle of asteroid Vesta: Assessing the effects of large, young craters. *Icarus* 244:74–88. doi:10.1016/j.icarus.2014.01.033.

Wisdom J. 1987. Chaotic dynamics in the solar system. *Icarus* 72:241–275. doi:10.1016/0019-1035(87)90175-8.

Yamashita N., Prettyman T. H., Mittlefehldt D. W., Toplis M. J., McCoy T. J., Beck A. W., Reedy R. C., Feldman W. C., Lawrence D. J., Peplowski P. N., Forni O., Mizzon H., Raymond C. A., and Russell C. T. 2013. Distribution of iron on Vesta. *Meteoritics & Planetary Science* 48:2237–2251. doi:10.1111/maps.12139.